Journal of Computational Physics **160,** 241–282 (2000)
doi:10.1006/jcph.2000.6459, available online at http://www.idealibrary.com on IDEAL®

New High-Resolution Central Schemes for Nonlinear Conservation Laws and Convection–Diffusion Equations

Alexander Kurganov* and Eitan Tadmor†

*Department of Mathematics, University of Michigan, Ann Arbor, Michigan 48109; and †Department of Mathematics, UCLA, Los Angeles, California 90095
E-mail: *kurganov@math.lsa.umich.edu, †tadmor@math.ucla.edu

Received April 8, 1999; revised December 8, 1999

Central schemes may serve as universal finite-difference methods for solving nonlinear convection–diffusion equations in the sense that they are not tied to the specific eigenstructure of the problem, and hence can be implemented in a straightforward manner as black-box solvers for general conservation laws and related equations governing the spontaneous evolution of large gradient phenomena. The first-order Lax–Friedrichs scheme (P. D. Lax, 1954) is the forerunner for such central schemes. The central Nessyahu–Tadmor (NT) scheme (H. Nessyahu and E. Tadmor, 1990) offers higher resolution while retaining the simplicity of the Riemann-solver-free approach. The numerical viscosity present in these central schemes is of order $\mathcal{O}((\Delta x)^{2r}/\Delta t)$. In the convective regime where $\Delta t \sim \Delta x$, the improved resolution of the NT scheme and its generalizations is achieved by lowering the amount of numerical viscosity with increasing r. At the same time, this family of central schemes suffers from excessive numerical viscosity when a sufficiently small time step is enforced, e.g., due to the presence of degenerate diffusion terms.

In this paper we introduce a new family of central schemes which retain the simplicity of being independent of the eigenstructure of the problem, yet which enjoy a much smaller numerical viscosity (of the corresponding order $\mathcal{O}(\Delta x)^{2r-1}$)). In particular, our new central schemes maintain their high-resolution independent of $\mathcal{O}(1/\Delta t)$, and letting $\Delta t \downarrow 0$, they admit a particularly simple semi-discrete formulation. The main idea behind the construction of these central schemes is the use of more precise information of the local propagation speeds. Beyond these CFL related speeds, no characteristic information is required. As a second ingredient in their construction, these central schemes realize the (nonsmooth part of the) approximate solution in terms of its cell averages integrated over the Riemann fans of varying size.

The semi-discrete central scheme is then extended to multidimensional problems, with or without degenerate diffusive terms. Fully discrete versions are obtained with

0021-9991/00 $35.00

Runge–Kutta solvers. We prove that a scalar version of our high-resolution central scheme is nonoscillatory in the sense of satisfying the total-variation diminishing property in the one-dimensional case and the maximum principle in two-space dimensions. We conclude with a series of numerical examples, considering convex and nonconvex problems with and without degenerate diffusion, and scalar and systems of equations in one- and two-space dimensions. Time evolution is carried out by the third- and fourth-order explicit embedded integration Runge–Kutta methods recently proposed by A. Medovikov (1998). These numerical studies demonstrate the remarkable resolution of our new family of central scheme.

Key Words: hyperbolic conservation laws; multidimensional systems; degenerate diffusion; central difference schemes; non-oscillatory time differencing.

CONTENTS

1. INTRODUCTION

During the past few decades there has been an enormous amount of activity related to the construction of approximate solutions for nonlinear conservation laws,

$$\frac{\partial}{\partial t}u(x,t)+\frac{\partial}{\partial x}f(u(x,t))=0, \tag{1.1}$$

and for the closely related convection–diffusion equations,

$$\frac{\partial}{\partial t}u(x,t)+\frac{\partial}{\partial x}f(u(x,t))=\frac{\partial}{\partial x}Q[u(x,t),u_x(x,t)]. \tag{1.2}$$

Here, $u(x,t)=(u_1(x,t),\dots,u_N(x,t))$ is an N-vector of conserved quantities, $f(u)$ is a nonlinear convection flux, and $Q(u,u_x)$ is a dissipation flux satisfying the (weak) parabolicity condition $\nabla_s Q(u,s)\ge 0\ \forall u,s$. In the general multidimensional case u is an N-vector in the d-spatial variables $x=(x_1,\dots,x_d)$, with the corresponding fluxes $f(u)=(f^1,\dots,f^d)$ and $Q(u,\nabla_x u)=(Q^1,\dots,Q^d)$.

These equations are of great practical importance since they govern a variety of physical phenomena that appear in fluid mechanics, astrophysics, groundwater flow, meterology, semiconductors, and reactive flows. Convection–diffusion equations (1.2) also arise in two-phase flow in oil reservoirs, non-Newtonian flows, front propagation, traffic flow, financial modeling, and several other areas.

In this work we present new second-order central difference approximations to (1.1) and (1.2). These new schemes can be viewed as modifications of the Nessyahu–Tadmor (NT) scheme [38]. Our schemes enjoy the major advantages of the central schemes over

the upwind ones: first, no Riemann solvers are involved, and second—as a result of being Riemann solver free—their realization and generalization for complicated multidimensional systems (1.1) and (1.2) are considerably simpler than in the upwind case. At the same time, the new schemes have a smaller amount of numerical viscosity than the original NT scheme, and unlike other central schemes, they can be written and efficiently integrated in their semi-discrete form.

We would like to emphasize the importance of semi-discrete formulations for solving "real," practical problems associated with multidimensional systems (1.1) and (1.2). Semi-discrete schemes are especially effective when they combine *high-resolution, non-oscillatory spatial discretization* with high-order, large stepsize ODE solvers for their time evolution.

The advantage of our semi-discrete scheme is clearly demonstrated later, in Figs. 6.21 and 6.22, where it is compared with the fully discrete NT solution of the degenerate convection–diffusion equation.

$$u_t + f(u)_x = \left(\frac{u_x}{\sqrt{1+u_x^2}} \right)_x. \tag{1.3}$$

This model, recently proposed in [28], describes high-gradient phenomena with possible discontinuous subshock solutions; consult [12, 28] for details. When the NT scheme is used to resolve these discontinuities, the computed subshocks are smeared due to the larger numerical dissipation which is accumulated ove the small time steps enforced by the restricted CFL stability condition, $\Delta t \sim (\Delta x)^2$. This situation—of excessive numerical dissipation (of order $\mathcal{O}((\Delta x)^{2r}/\Delta t)$)—is typical for fully discrete central schemes with time steps much smaller than the convective CFL limitation. Alternatively, our new central scheme will accumulate less dissipation (of order $\mathcal{O}(\Delta x)^{2r-1}$) and hence can be efficiently used with time steps as small as required.

This paper is organized as follows. In Section 2 we provide a brief description of the central differencing approach for hyperbolic conservation laws.

In Section 3 we introduce our new fully discrete second-order central scheme, which is constructed for systems of one-dimensional hyperbolic conservation laws. The limiting case, $\Delta t \downarrow 0$, brings us to the semi-discrete version presented in Subsection 4.1. Here we prove that our second-order semi-discrete central scheme satisfies the scalar total-variation diminishing (TVD) property; consult Theorem 4.1 below. In Subsections 4.2 and 4.3 our semi-discrete scheme is extended, respectively, to one-dimensional convection–diffusion equations and to multidimensional hyperbolic and (degenerate) parabolic problems.

In Section 5 we return to the fully discrete framework, discussing time discretization for our semi-discrete central scheme. Specifically, we use efficient Runge–Kutta ODE solvers to integrate the semi-discrete schemes outlined earlier in Section 4. We retain the overall Riemann-free simplicity without giving up high resolution. Here we prove that the resulting second-order fully discrete central scheme satisfies the scalar the maximum principle; consult Theorem 5.1.

We end in Section 6 by presenting a number of numerical results. These results are convincing illustrations that our new central schemes provide high resolution at a lowest cost, when applied both to hyperbolic systems of conservation laws and to a variety of convection–diffusion models. These numerical results confirm an essential aspect of the current approach—retaining high-resolution *without* the costly (approximate) Riemann

solvers, characteritic decompositions, etc. This aspect in the context of high-resolution schemes was introduced in the Nessyahu–Tadmor scheme [38] and was extended to two-dimensional problems in [18]. A nonstaggered and hence less dissipative version was presented in [17]. The relaxation scheme introduced in [19] is closely related to these staggered central schemes; in fact, they coicide in the relaxation limit $\varepsilon \downarrow 0$. The choice for a relaxation *matrix* A in [19] provides us a *family* of high-resolution schemes; we note in passing that the special scalar choice $A = \rho(\partial f(u)/\partial u)I$ is an $\mathcal{O}(\varepsilon)$ perturbation of the central scheme discussed in this paper. Other componentwise approaches were presented in [34]. The CUSP scheme presented in [16] is a semi-discrete scheme which avoids characteristic decompositions. And more recently, Liu and Osher [35] introduced a semi-discrete scheme based on a pointwise formulation of ENO which retains high resolution without Riemann solvers.

2. CENTRAL SCHEMES—A BRIEF OVERVIEW

Central schemes offer universal finite-difference methods for solving hyperbolic conservation laws, in the sense that they are not tied up to the specific eigenstructure of the problem and hence can be implemented in a straightforward manner as a black-box solver for general systems (1.1). In particular, they do not involve characteristic decomposition of the flux f. In fact, even computation of the Jacobian of f can be avoided; in the particular case of the second-order NT scheme, for example, numerical derivatives of the flux in (2.6) below can be implemented componentwise—consult [18, 36].

In 1954 Lax and Friedrichs [10, 29] introduced the first-order stable central scheme, the celebrated Lax–Friedrichs (LxF) scheme:

$$u_j^{n+1} = \frac{u_{j+1}^n + u_{j-1}^n}{2} - \frac{\lambda}{2}\left[f\left(u_{j+1}^n\right) - f\left(u_{j-1}^n\right)\right]. \tag{2.1}$$

Here, $\lambda := \Delta t/\Delta x$ is the fixed mesh ratio, and u_j^n is an approximate value of $u(x = x_j, t = t^n)$ at the grid point $(x_j := j\Delta x, t^n := n\Delta t)$. Compared with the canonical first-order upwind scheme of Godunov [11], the central LxF scheme has the advantage of *simplicity*, since no (approximate) Riemann solvers, e.g., [42], are involved in its construction. The main disadvantage of the LxF scheme, however, lies in its large numerical dissipation, which prevents sharp resolution of shock discontinuities and rarefaction tips.

A natural high-order extension of the LxF scheme—the NT scheme—was presented in 1990 in [38]. The main idea of this generalization is replacing the first-order piecewise constant solution which is behind the original LxF scheme with van Leer's MUSCL-type piecewise-linear second-order approximation, e.g., [31]. This is then combined with a *LxF solver*—an alternative to the upwind solvers, which avoids the time-consuming resolution of Riemann fans by staggered (x, t)-integration. Thus, the NT scheme retains the simplicity of the Riemann-free LxF framework while gaining high resolution, which eliminates the disadvantage of excessive first-order dissipation.

Here is a brief readers' digest based on the representation of the LxF and NT schemes as Godunov-type schemes. We follow [36, Section 2]. To this end, we utilize the sliding average of $u(\cdot, t)$,

$$\bar{u}(x,t) := \frac{1}{|I_x|}\int\limits_{I_x} u(\xi,t)\,d\xi, \qquad I_x := \left\{\xi : |\xi - x| \le \frac{\Delta x}{2}\right\},$$

so that the integration of (1.1) over the rectangle $I_x \times [t, t+\Delta t]$ yields an equivalent reformulation of the conservation law, (1.1),

$$\bar{u}(x, t+\Delta t) = \bar{u}(x,t) - \frac{1}{\Delta x}\left[\int_{\tau=t}^{t+\Delta t} f\left(u\left(x+\frac{\Delta x}{2}, \tau\right)\right)d\tau - \int_{\tau=t}^{t+\Delta t} f\left(u\left(x-\frac{\Delta x}{2}, \tau\right)\right)d\tau\right]. \tag{2.2}$$

We begin by assuming that we have already computed an approximation to the solution at time level $t = t^n$—a piecewise linear approximation $\tilde{u}(x, t^n) \approx u(x, t^n)$ of the form

$$\tilde{u}(x, t^n) := \sum_j \left[\bar{u}_j^n + (u_x)_j^n (x - x_j)\right]\mathbf{1}_{[x_{j-1/2}, x_{j+1/2}]}, \qquad x_{j\pm 1/2} := x_j \pm \frac{\Delta x}{2}. \tag{2.3}$$

Here, $\{\bar{u}_j^n\}$ are the computed cell averages, $\bar{u}_j^n \approx \bar{u}(x_j, t^n) = \int_{I_{x_j}} u(\xi, t^n)\, d\xi/\Delta x$, and $\{(u_x)_j^n\}$ are approximations to the exact derivatives, $u_x(x_j, t^n)$. These approximate derivatives are *reconstructed* from the computed cell averages. The nonoscillatory behavior of the central schemes hinges on the appropriate choice of approximate derivatives, and there is a library of recipes for such nonoscillatory reconstructions. A total-variation (TV) stability, a maximum principle, or a weaker nonoscillatory property of this piecewise-linear approximation (e.g., decreasing the number of extrema [36, Section 4]) can be satisfied for a wide variety of such scalar reconstructions proposed and discussed in [4, 13, 14, 27, 32, 36, 38, 41]. For example, a scalar TVD reconstruction in (2.3) is obtained via the ubiquitous *minmod limiter* [13, 31, 41],

$$(u_x)_j^n = \text{minmod}\left(\frac{u_j^n - u_{j-1}^n}{\Delta x}, \frac{u_{j+1}^n - u_j^n}{\Delta x}\right), \tag{2.4}$$

with $\text{minmod}(a, b) := \frac{1}{2}[\text{sgn}(a) + \text{sgn}(b)] \cdot \min(|a|, |b|)$. This is a particular case of a one-parameter family of limiters outlined in (5.2) below.

We then proceed to solve Eq. (2.2) subject to the piecewise-linear initial data (2.3) depicted in Fig. 2.1.

The piecewise-linear interpolant, $\tilde{u}(x, t^n)$, may be discontinuous at points $\{x_{j+1/2}\}$. Yet for sufficiently small Δt, the solution of problem (2.2)–(2.3) will remain smooth around x_j for $t \le t^n + \Delta t =: t^{n+1}$, due to the finite speed of propagation. Hence, if we take I_x to be the staggered grid cell, $[x_j, x_{j+1}]$ (see Fig. 2.1), we can compute $\bar{u}(x, t)$ on the RHS of (2.2) exactly, and the flux integrals there can be approximated by the midpoint rule. This results in the NT scheme [38]

$$\bar{u}_{j+1/2}^{n+1} = \frac{\bar{u}_j^n + \bar{u}_{j+1}^n}{2} + \frac{\Delta x}{8}\left((u_x)_j^n - (u_x)_{j+1}^n\right) - \lambda\left[f\left(u_{j+1}^{n+1/2}\right) - f\left(u_j^{n+1/2}\right)\right], \tag{2.5}$$

where the midpoint values, $u_j^{n+1/2}$, are predicted by Taylor expansion,

$$u_j^{n+1/2} = \bar{u}_j^n - \frac{\Delta t}{2}(f_x)_j^n. \tag{2.6}$$

Thus, we have computed an approximate solution at the next time level $t = t^{n+1}$, a solution which is realized by its (staggered) cell averages, $\bar{u}_{j+1/2}^{n+1}$.

Extensions of the second order central NT scheme (2.5), (2.6) to higher-order central schemes can be found in [4, 32, 36]. Multidimensional extensions were introduced in

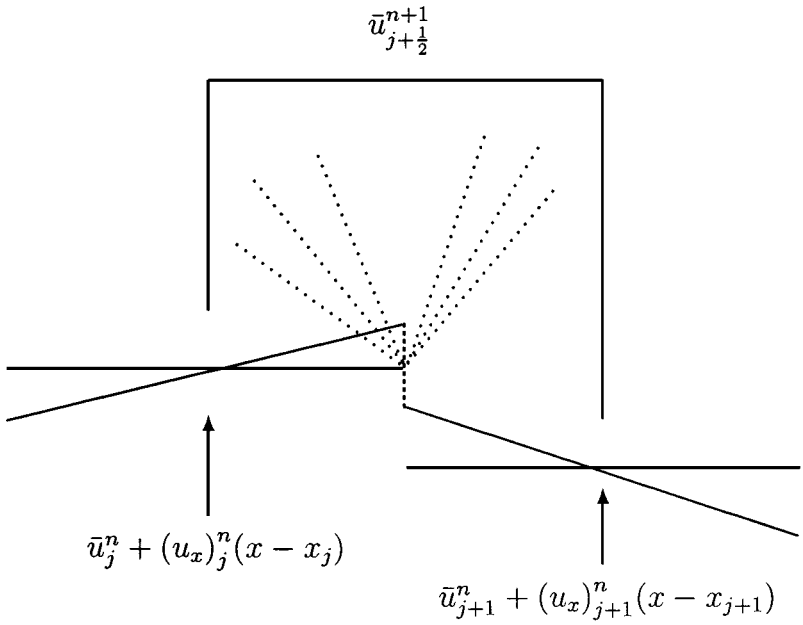

FIG. 2.1. Central differencing approach—staggered integration over the local Riemann fan.

[2, 3, 18]. We also would like to mention the corresponding central schemes for incompressible flows in [24–26, 33] and applications to various systems in, e.g., [1, 7, 43]. Thus, the use of higher-order reconstructions enables us to decrease the numerical dissipation present in central schemes, and achieve a higher resolution of shocks, rarefactions, and other spontaneous evolution of large gradient phenomena.

Remarks. 1. Characteristic vs componentwise approach. A key advantage of central schemes is their simplicity–one avoids here the intricate and time-consuming characteristic decompositions based on (approximate) Riemann solvers, which are necessary in high-resolution upwind formulations. For systems of conservation laws, the numerical derivatives $(u_x)^n_j$ can be implemented by *componentwise* extension of the scalar recipe for nonoscillatory limiters. Similarly, the predicted values in (2.6) are based on approximate derivatives of the flux, $(f_x)^n_j$. These values can be computed in terms of the exact Jacobian, $\frac{\partial f}{\partial u}(\bar{u}^n_j)(u_x)^n_j$. Alternatively, we can even avoid the use of the computationally expensive (and sometimes inaccessible) exact Jacobian $\frac{\partial f}{\partial u}$. Instead, the approximate flux derivatives, $(f_x)^n_j$, are computed in a componentwise manner based on the neighboring discrete values of $f(\bar{u}(x_{j-1}, t^n))$, $f(\bar{u}(x_j, t^n))$ and $f(\bar{u}(x_{j+1}, t^n))$. It was pointed out in [36, 18] that this Jacobian-free version of the central scheme does not deteriorate its high resolution.

2. *Cell averages vs point values.* Note that here one realizes the approximate solution by its cell averages, $\bar{u}^{n+1}_{j+1/2}$. In general, when dealing with first- and second-order schemes, the cell averages, $\bar{u}^{n+1}_{j+1/2}$, can be identified with the corresponding point values, $u^{n+1}_{j+1/2}$, modulo a negligible second-order term. We therefore from now on omit the bar notation. (Consult [4, 36], for example, for this distinction with higher-order central schemes).

3. *Second- vs first-order.* In the particular case of $(u_x)^n_j \equiv 0$, the second-order NT scheme is reduced to the staggered form of the first-order LxF scheme. The nonstaggered version of a second-order central scheme can be found in [17].

The second-order NT scheme and its extensions owe their superior resolution to the lower amount of numerical dissipation—considerably lower than in the first-order LxF scheme. The dissipation present in these central scheme has an amplitude of order $\mathcal{O}((\Delta x)^{2r}/\Delta t)$; unfortunately, this does not circumvent the difficulties with small time steps which arise, e.g., with convection–diffusion equations (1.2). Consider, for example, the *degenerate parabolic* equation (1.3). Stability necessitates small time steps, $\Delta t \sim (\Delta x)^2$, and the influence of the numerical dissipation, *accumulated* over the many steps of the NT scheme, can be clearly seen in the smeared subshock computed in Fig. 6.22.

One possible way to overcome this difficulty is to use a *semi-discrete* formulation: when a semi-discrete scheme is coupled with an appropriate ODE solver, one ends up with small numerical viscosity proportional to the vanishing size of the time step Δt. But in this context, the central LxF scheme, NT scheme, and their extensions are of limited use, since these schemes do not admit a *semi-discrete form*. To make our point, consider the LxF scheme (2.1) in its viscous form,

$$\frac{u_j^{n+1}-u_j^n}{\Delta t}+\frac{f\left(u_{j+1}^n\right)-f\left(u_{j-1}^n\right)}{2\Delta x}=\frac{1}{2\Delta t}\left[\left(u_{j+1}^n-u_j^n\right)-\left(u_j^n-u_{j-1}^n\right)\right]. \quad (2.7)$$

Passing to the limit $\Delta t \to 0$ (while leaving Δx to be fixed), we get the semi-discrete divergence on the left of (2.7), $\dot{u}_j(t)+\{f(u_{j+1}(t))-f(u_{j-1}(t))\}/2\Delta x$, which is balanced with an increasing amount of dissipation on the right $\sim u_{xx}(\Delta x)^2/\Delta t \uparrow \infty$, as we refine the time step $\Delta t \downarrow 0$. In the degenerate viscous case, for example, the CFL restriction $\Delta t \ll \Delta x$ is responsible for the excessive smearing in the LxF scheme. The second-order NT scheme has a considerably smaller numerical viscosity, with amplitude of order $\mathcal{O}((\Delta x)^4/\Delta t)$ away from extrema cells.[1] Nevertheless, the central NT scheme and its higher-order generalizations do not admit any semi-discrete versions, and hence are inappropriate for small time step computations or steady-state calculations as $t \uparrow \infty$.

This brings us to the new class of central schemes introduced in this paper. These new central schemes have smaller numerical dissipation and are the first fully discrete Godunov-type central schemes that admit a semi-discrete form.

3. THE FULLY DISCRETE SCHEME—ONE-DIMENSIONAL SETUP

The NT scheme is based on averaging over the nonsmooth Riemann fans using spatial cells of the *fixed* width, Δx. The main idea in the construction of our new central schemes is to use more precise information about the *local* speed of wave propagation, in order to average the nonsmooth parts of the computed solution over smaller cells of variable size of order $\mathcal{O}(\Delta t)$. We proceed as follows.

Assume that we have already computed the piecewise-linear solution at time level t^n, based on the cell averages u_j^n, and have reconstructed approximate derivatives $(u_x)_j^n$ in (2.3). We now turn to evolve it in time. To begin with, we estimate the local speed of propagation at the cell boundaries, $x_{j+1/2}$: the upper bound (disregarding the direction of the propagation)

[1] The first two terms on the right of the NT scheme (2.5) yield for smooth u's

$$\frac{\overline{u}_j^n-2\overline{u}_{j+1/2}^n+\overline{u}_{j+1}^n}{2\Delta t}+\frac{\Delta x}{8\Delta t}\left((u_x)_j^n-(u_x)_{j+1}^n\right)\sim\frac{(\Delta x)^4}{\Delta t}u_{xxxx}.$$

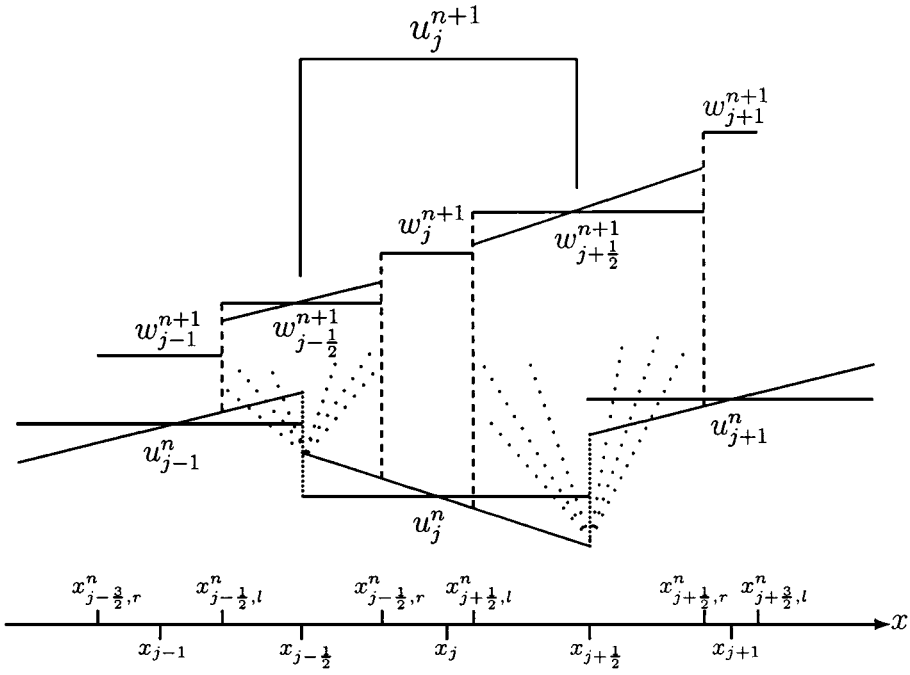

FIG. 3.2. Modified central differencing.

is denoted by $a_{j+1/2}^n$ and is given by[2]

$$a_{j+1/2}^n = \max_{u\in\mathcal{C}(u_{j+1/2}^-,u_{j+1/2}^+)} \rho\left(\frac{\partial f}{\partial u}(u)\right), \tag{3.1}$$

where $u_{j+1/2}^+ := u_{j+1}^n - \frac{\Delta x}{2}(u_x)_{j+1}^n$ and $u_{j+1/2}^- := u_j^n + \frac{\Delta x}{2}(u_x)_j^n$ are the correspondent left and right intermediate values of $\tilde{u}(x, t^n)$ at $x_{j+1/2}$, and $\mathcal{C}(u_{j+1/2}^-, u_{j+1/2}^+)$ is a curve in phase space connecting $u_{j+1/2}^-$ and $u_{j+1/2}^+$ via the Riemann fan.

Remark. In most practical applications, these local maximal speeds can be easily evaluated. For example, in the genuinely nonlinear or linearly degenerate case one finds that (3.1) reduces to

$$a_{j+1/2}^n := \max\left\{\rho\left(\frac{\partial f}{\partial u}\left(u_{j+1/2}^-\right)\right), \rho\left(\frac{\partial f}{\partial u}\left(u_{j+1/2}^+\right)\right)\right\}. \tag{3.2}$$

In fact, the maximal local speeds are related to the already calculated CFL number. We emphasize that these local speeds are the only additional information required to modify the NT scheme.

Our new scheme is constructed in two steps. First, we proceed along the lines of the NT scheme. The NT scheme is based on averaging over the staggered control volumes $[x_j, x_{j+1}] \times [t^n, t^{n+1}]$ of fixed spatial width Δx. Instead, we now use narrower control volumes, where at each time step we integrate over the intervals $[x_{j+1/2,l}^n, x_{j+1/2,r}^n] \times [t^n, t^{n+1}]$; see Fig. 3.2. Due to the finite speed of propagation, the points $x_{j+1/2,l}^n := x_{j+1/2} - a_{j+1/2,}^n \Delta t$ and $x_{j+1/2,r}^n := x_{j+1/2} + a_{j+1/2}^n \Delta t$ separate between smooth and nonsmooth regions, and

[2] Let $\lambda_i(A)$ be the eigenvalues of A; then we use $\rho(A) := \max_i |\lambda_i(A)|$ to denote its spectral radius.

hence the nonsmooth parts of the solution are contained inside these narrower control volumes of spatial width $2a^n_{j+1/2}\Delta t$.

We proceed with the exact evaluation of the new cell averages at t^{n+1}. Let $\Delta x_{j+1/2} := x^n_{j+1/2,r} - x^n_{j+1/2,l}$ denote the width of the Riemann fan which originates at $x_{j+1/2}$. Exact computation of the spatial integrals yields

$$\begin{aligned}
&\frac{1}{\Delta x_{j+1/2}} \int_{x^n_{j+1/2,l}}^{x^n_{j+1/2,r}} u(\xi, t^{n+1})\, d\xi \\
&= \frac{1}{\Delta x_{j+1/2}} \int_{x^n_{j+1/2,l}}^{x^n_{j+1/2,r}} \tilde{u}(\xi, t^n)\, d\xi - \frac{1}{\Delta x_{j+1/2}} \int_{t^n}^{t^{n+1}} \left[f\left(u\left(x^n_{j+1/2,r}, \tau\right)\right) - f\left(u\left(x^n_{j+1/2,l}, \tau\right)\right)\right] d\tau \\
&= \frac{u^n_j + u^n_{j+1}}{2} + \frac{\Delta x - a^n_{j+1/2}\Delta t}{4}\left((u_x)^n_j - (u_x)^n_{j+1}\right) \\
&\quad - \frac{1}{2a^n_{j+1/2}\Delta t} \int_{t^n}^{t^{n+1}} \left[f\left(u\left(x^n_{j+1/2,r}, \tau\right)\right) - f\left(u\left(x^n_{j+1/2,l}, \tau\right)\right)\right] d\tau. \qquad (3.3)
\end{aligned}$$

Similarly, let $\Delta x_j := x^n_{j+1/2,l} - x^n_{j-1/2,r} = \Delta x - \Delta t(a^n_{j-1/2} + a^n_{j+1/2})$ denote the width of strip around x_j which is free of the neighboring Riemann fans. Then exact integration yields

$$\begin{aligned}
&\frac{1}{\Delta x_j} \int_{x^n_{j-1/2,r}}^{x^n_{j+1/2,l}} u(\xi, t^{n+1})\, d\xi \\
&= \frac{1}{\Delta x_j} \int_{x^n_{j-1/2,r}}^{x^n_{j+1/2,l}} \tilde{u}(\xi, t^n)\, d\xi - \frac{1}{\Delta x_j} \int_{t^n}^{t^{n+1}} \left[f\left(u\left(x^n_{j+1/2,l}, \tau\right)\right) d\tau - f\left(u\left(x^n_{j-1/2,r}, \tau\right)\right)\right] d\tau \\
&= u^n_j + \frac{\Delta t}{4}\left(a^n_{j-1/2} - a^n_{j+1/2}\right)(u_x)^n_j \\
&\quad - \frac{1}{\Delta x_j} \int_{t^n}^{t^{n+1}} \left[f\left(u\left(x^n_{j+1/2,l}, \tau\right)\right) - f\left(u\left(x^n_{j-1/2,r}, \tau\right)\right)\right] d\tau. \qquad (3.4)
\end{aligned}$$

Using the midpoint rule to approximate the flux integrals on the RHS of (3.3) and (3.4), we conclude with the new cell averages at $t = t^{n+1}$,

$$\begin{aligned}
w^{n+1}_{j+1/2} &= \frac{u^n_j + u^n_{j+1}}{2} + \frac{\Delta x - a^n_{j+1/2}\Delta t}{4}\left((u_x)^n_j - (u_x)^n_{j+1}\right) \\
&\quad - \frac{1}{2a^n_{j+1/2}}\left[f\left(u^{n+1/2}_{j+1/2,r}\right) - f\left(u^{n+1/2}_{j+1/2,l}\right)\right], \\
w^{n+1}_j &= u^n_j + \frac{\Delta t}{2}\left(a^n_{j-1/2} - a^n_{j+1/2}\right)(u_x)^n_j \\
&\quad - \frac{\lambda}{1 - \lambda\left(a^n_{j-1/2} + a^n_{j+1/2}\right)}\left[f\left(u^{n+1/2}_{j+1/2,l}\right) - f\left(u^{n+1/2}_{j-1/2,r}\right)\right].
\end{aligned} \qquad (3.5)$$

Here, the midpoint values are obtained from the corresponding Taylor expansions,

$$u^{n+1/2}_{j+1/2,l} := u^n_{j+1/2,l} - \frac{\Delta t}{2} f\left(u^n_{j+1/2,l}\right)_x, \qquad u^n_{j+1/2,l} := u^n_j + \Delta x (u_x)^n_j \left(\frac{1}{2} - \lambda a^n_{j+1/2}\right),$$

$$u^{n+1/2}_{j+1/2,r} := u^n_{j+1/2,r} - \frac{\Delta t}{2} f\left(u^n_{j+1/2,r}\right)_x, \qquad u^n_{j+1/2,r} := u^n_{j+1} - \Delta x (u_x)^n_{j+1} \left(\frac{1}{2} - \lambda a^n_{j+1/2}\right). \tag{3.6}$$

Again, if we want to, we can avoid the computation of the Jacobian of f while using a componentwise evaluation of f_x on the right of (3.6).

At this stage, we realize the solution at time level $t = t^{n+1}$ in terms of the approximate cell averages, $w^{n+1}_{j+1/2}$, w^{n+1}_j. These averages spread over a nonuniform grid which is oversampled by twice the number of the original cells at $t = t^n$. In the second and final step of the construction of our scheme, we *convert* these nonuniform averages back into the original grid we started with at $t = t^n$, along the lines of the conversion recipe outlined in [17]. As a by-product of this conversion, we avoid the staggered form of the original NT scheme (2.5)–(2.6).

To obtain the cell averages over the original grid of the uniform, nonstaggered cells $[x_{j-1/2}, x_{j+1/2}]$, we consider the piecewise-linear reconstruction over the nonuniform cells at $t = t^{n+1}$, and following [17], we project its averages back onto the original uniform grid. Note that we do not need to reconstruct the average of the smooth portion of the solution, w^{n+1}_j, as it will be averaged out (consult Fig. 3.2), and hence the required piecewise-linear approximation takes the form

$$\tilde{w}(x, t^{n+1}) := \sum_j \Big\{\big[w^{n+1}_{j+1/2} + (u_x)^{n+1}_{j+1/2}\big(x - x_{j+1/2}\big)\big]\mathbf{1}_{[x^n_{j+1/2,l}, x^n_{j+1/2,r}]} + w^{n+1}_j \mathbf{1}_{[x^n_{j-1/2,r}, x^n_{j+1/2,l}]}\Big\}. \tag{3.7}$$

Here, the exact spatial derivatives, $u_x(x_{j+1/2}, t^{n+1})$, are approximated by

$$(u_x)^{n+1}_{j+1/2} = \frac{2}{\Delta x} \cdot \operatorname{minmod}\left(\frac{w^{n+1}_{j+1} - w^{n+1}_{j+1/2}}{1 + \lambda\big(a^n_{j+1/2} - a^n_{j+3/2}\big)}, \frac{w^{n+1}_{j+1/2} - w^{n+1}_j}{1 + \lambda\big(a^n_{j+1/2} - a^n_{j-1/2}\big)}\right). \tag{3.8}$$

Finally, the desired cell averages, u^{n+1}_j, are obtained by averaging the approximate solution in (3.7). Our *fully discrete second-order* central scheme then recasts into the final form

$$u^{n+1}_j = \frac{1}{\Delta x}\int\limits_{x_{j-1/2}}^{x_{j+1/2}} \tilde{w}(\xi, t^{n+1})\, d\xi = \lambda a^n_{j-1/2} w^{n+1}_{j-1/2} + \big[1 - \lambda\big(a^n_{j-1/2} + a^n_{j+1/2}\big)\big]\, w^{n+1}_j + \lambda a^n_{j+1/2}\, w^{n+1}_{j+1/2} + \frac{\Delta x}{2}\big[\big(\lambda a^n_{j-1/2}\big)^2 (u_x)^{n+1}_{j-1/2} - \big(\lambda a^n_{j+1/2}\big)^2 (u_x)^{n+1}_{j+1/2}\big], \tag{3.9}$$

where the intermediate values of $w^{n+1}_{j+1/2}$ and w^{n+1}_j specified in (3.5) are expressed in terms of the local speed, $a^n_{j\pm1/2}$, the midvalues, $u^{n+1/2}_{j+1/2,l}, u^{n+1/2}_{j+1/2,r}$, and the reconstructed slopes, $(u_x)^{n+1}_{j\pm1/2}$, given in (3.2), (3.6), and (3.8), respectively.

Remarks. 1. *Central differencing.* The approach taken here can be still viewed as central differencing in the sense that the Riemann fans are inside the domain of averaging. Consequently, since no (approximate) Riemann solvers are involved, we retain one of the main advantages of the central schemes—simplicity; no Jacobians and charactristic decompositions are needed. At the same time, treating smooth and nonsmooth regions separately, we gain smaller numerical viscosity (independent of $\mathcal{O}(1/\Delta t)$). In particular, the resulting central scheme (3.9), (3.5) admits a semi-discrete form which is discussed in the next section.

2. *Nonoscillatory properties.* The exact entropy evolution operator associated with the scalar equation satisfies the TVD property, $\|u(\cdot,t)\|_{BV} \le \|u(\cdot,0)\|_{BV}$. The various ingredients in the construction of our central scheme retain this TVD property—the nonoscillatory reconstruction (with appropriate choice of approximate derivatives), exact evolution, and cell averaging. Thus, the *only* ingredient that is potentially oscillatory enters when we use the midpoint quadrature rule for temporal integration of the fluxes, yet this does not seem to violate the overall TVD property of our fully discrete central scheme; see, e.g., the TVD proof of the original NT scheme in [38].

In the particular semi-discrete case (discussed in Section 4 below), the midpoint rule is "exact," and the TVD of the semi-discrete version of our scheme follows. A direct proof for the semi-discrete scalar TVD is outlined in Theorem 4.1 below. Moreover, when this semi-discrete scheme is coupled with appropriate Runge–Kutta solvers, we arrive at fully discrete, second-order, central TVD schemes; consult Section 5 below. A maximum principle for these schemes in two-space dimensions is outlined in Theorem 5.1.

3. *Nonstaggered reconstruction.* The piecewise linear reconstruction, (3.7), is necessary in order to ensure second-order accuracy, since simple averaging (without reconstruction) over $[x_{j-1/2}, x_{j+1/2}]$ reduces the order of the resulting scheme to first-order accuracy; see [17].

4. *First-order version.* We conclude by commenting on the first-order version of our scheme. To this end, we set the slopes, both $(u_x)_j^n$ and $(u_x)_{j+1/2}^{n+1}$, to be zero. Then the staggered cell averages in (3.5) are reduced to

$$w_{j+1/2}^{n+1} = \frac{u_j^n + u_{j+1}^n}{2} - \frac{1}{2a_{j+1/2}^n}\left[f\left(u_{j+1}^n\right) - f\left(u_j^n\right)\right], \qquad w_j^{n+1} = u_j^n.$$

Inserting these values into (3.9) yields the first-order scheme, which takes the viscous form

$$u_j^{n+1} = u_j^n - \frac{\lambda}{2}\left[f\left(u_{j+1}^n\right) - f\left(u_{j-1}^n\right)\right] + \frac{1}{2}\left[\lambda a_{j+1/2}^n\left(u_{j+1}^n - u_j^n\right) - \lambda a_{j-1/2}^n\left(u_j^n - u_{j-1}^n\right)\right], \tag{3.10}$$

where $a_{j+1/2}^n$ are the maximal local speeds. This scheme was originally attributed to Rusanov [30]; it is a special case of the family of first-order Godunov-type scheme introduced in [15] (based on a symmetric approximate Rieman solver) and it coincides with the so-called local LxF scheme in [45]. It should be noted, however, that although this scheme is similar to the LxF scheme, (2.7), its numerical viscosity coefficient, $Q_{j+1/2}^n = \lambda a_{j+1/2}^n$, is always smaller than the corresponding LxF one, $Q_{j+1/2}^{\mathrm{LxF}} \equiv 1$, thanks to the CFL condition. In regions with a small local speed of propagation (e.g., near the sonic points), the numerical viscosity present in (3.10) is in fact considerably smaller, $\Delta t a_{j+1/2}^n \ll \Delta x$.

4. THE REDUCTION TO SEMI-DISCRETE FORMULATION

4.1. *One-Dimensional Hyperbolic Conservation Laws*

We consider the fully discrete second-order central scheme (3.9), (3.5), expressed in terms of the cell averages, $w^{n+1}_{j\pm1/2}$, w^{n+1}_j, and the approximate derivates, $(u_x)^{n+1}_{j\pm1/2}$. Observe that except the original averages, u^n_j, which participates in w^n_j, *all* the terms on the right of (3.9), (3.5) are proportional to Δt (or λ). Rearranging the divided differences accordingly while separating the vanishing terms proportional to λ (as $\Delta t \downarrow 0$) we find

$$
\begin{aligned}
&\frac{u^{n+1}_j - u^n_j}{\Delta t}\\
&\overset{(3.9)}{\downarrow} \frac{a^n_{j-1/2}}{\Delta x} w^{n+1}_{j-1/2} + \left(\frac{1}{\Delta x} - \frac{a^n_{j-1/2} + a^n_{j+1/2}}{\Delta x}\right) w^{n+1}_j + \frac{a^n_{j+1/2}}{\Delta x} w^{n+1}_{j+1/2} - \frac{1}{\Delta t} u^n_j + \mathcal{O}(\lambda)\\
&\overset{(3.5)}{\downarrow} \left\{ \frac{a^n_{j-1/2}}{2\Delta x}\left(u^n_{j-1} + u^n_j\right) + \frac{1}{4} a^n_{j-1/2}\left((u_x)^n_{j-1} - (u_x)^n_j\right) - \frac{1}{2\Delta x}\left[f\left(u^{n+1/2}_{j-1/2,r}\right) - f\left(u^{n+1/2}_{j-1/2,l}\right)\right] \right.\\
&\quad - \frac{\left(a^n_{j-1/2} + a^n_{j+1/2}\right)}{\Delta x} u^n_j + \frac{1}{2}\left(a^n_{j-1/2} - a^n_{j+1/2}\right)(u_x)^n_j - \frac{1}{\Delta x}\left[f\left(u^{n+1/2}_{j+1/2,l}\right)\right.\\
&\quad \left. - f\left(u^{n+1/2}_{j-1/2,r}\right)\right] + \frac{a^n_{j+1/2}}{2\Delta x}\left(u^n_j + u^n_{j+1}\right) + \frac{1}{4} a^n_{j+1/2}\left((u_x)^n_j - (u_x)^n_{j+1}\right)\\
&\quad \left. - \frac{1}{2\Delta x}\left[f\left(u^{n+1/2}_{j+1/2,r}\right) - f\left(u^{n+1/2}_{j+1/2,l}\right)\right] \right\} + \mathcal{O}(\lambda)\\
&= \frac{1}{2\Delta x}\left\{ -\left[\left(f\left(u^{n+1/2}_{j+1/2,r}\right) + f\left(u^{n+1/2}_{j+1/2,l}\right)\right) - \left(f\left(u^{n+1/2}_{j-1/2,r}\right) + f\left(u^{n+1/2}_{j-1/2,l}\right)\right)\right] \right.\\
&\quad + \frac{a^n_{j+1/2}}{\Delta x}\left[\left(u^n_{j+1} - \frac{\Delta x}{2}(u_x)^n_{j+1}\right) - \left(u^n_j + \frac{\Delta x}{2}(u_x)^n_j\right)\right]\\
&\quad \left. - \frac{a^n_{j-1/2}}{\Delta x}\left[\left(u^n_j - \frac{\Delta x}{2}(u_x)^x_j\right) - \left(u^n_{j-1} + \frac{\Delta x}{2}(u_x)^n_{j-1}\right)\right]. \right\} + \mathcal{O}(\lambda).
\end{aligned}
$$

Note that as $\Delta t \to 0$, the midvalues on the right approach (consult (3.6))

$$
\begin{aligned}
u^{n+1/2}_{j+1/2,r} &\to u_{j+1}(t) - \frac{\Delta x}{2}(u_x)_{j+1}(t) =: u^+_{j+1/2}(t),\\
u^{n+1/2}_{j+1/2,l} &\to u_j(t) + \frac{\Delta x}{2}(u_x)_j(t) =: u^-_{j+1/2}(t),
\end{aligned}
\tag{4.1}
$$

where $(u_x)_j(t)$ are the numerical derivatives reconstructed from the computed cell averages, $u_j(t)$. Thus, letting $\Delta t \downarrow 0$, the resulting semi-discrete central scheme can be written in its compact form

$$
\begin{aligned}
\frac{d}{dt} u_j(t) = &-\frac{\left(f\left(u^+_{j+1/2}(t)\right) + f\left(u^-_{j+1/2}(t)\right)\right) - \left(f\left(u^+_{j-1/2}(t)\right) + \left(f\left(u^-_{j-1/2}(t)\right)\right)\right.}{2\Delta x}\\
&+ \frac{1}{2\Delta x}\left\{a_{j+1/2}(t)\left[u^+_{j+1/2}(t) - u^-_{j+1/2}(t)\right] - a_{j-1/2}(t)\left[u^+_{j-1/2}(t) - u^-_{j-1/2}(t)\right]\right\}.
\end{aligned}
\tag{4.2}
$$

Recall that $a_{j+1/2}(t)$ is the maximal local speed, e.g., in the generic case one may take

$$a_{j+1/2}(t) := \max\left\{\rho\left(\frac{\partial f}{\partial u}\left(u^+_{j+1/2}(t)\right)\right), \rho\left(\frac{\partial f}{\partial u}\left(u^-_{j+1/2}(t)\right)\right)\right\}.$$

Remarks. 1. *Conservation form.* The second-order scheme, (4.2), admits the conservative form,

$$\frac{d}{dt}u_j(t) = -\frac{H_{j+1/2}(t) - H_{j-1/2}(t)}{\Delta x}, \tag{4.3}$$

with the numerical flux

$$H_{j+1/2}(t) := \frac{f\left(u^+_{j+1/2}(t)\right) + f\left(u^-_{j+1/2}(t)\right)}{2} - \frac{a_{j+1/2}(t)}{2}\left[u^+_{j+1/2}(t) - u^-_{j+1/2}(t)\right]. \tag{4.4}$$

Here, the intermediate values $u^\pm_{j+1/2}$ are given by

$$u^+_{j+1/2} := u_{j+1}(t) - \frac{\Delta x}{2}(u_x)_{j+1}(t), \qquad u^-_{j+1/2} := u_j(t) + \frac{\Delta x}{2}(u_x)_j(t). \tag{4.5}$$

One verifies that $H_{j+1/2}(t) \equiv H(u_{j-1}(t), u_j(t), u_{j+1}(t), u_{j+2}(t))$ is a numerical flux consistent with Eq. (1.1), i.e., $H(v, v, v, v) = f(v)$. In fact, with the minmod limiter, (2.4), the corresponding approximate derivatives, $(u_x)_j(t)$, vanish at extrema values,

$$\operatorname{sgn}(u_{j+1}(t) - u_j(t)) + \operatorname{sgn}(u_j(t) - u_{j-1}(t)) = 0 \Rightarrow (u_x)_j(t) = 0, \tag{4.6}$$

and hence the corresponding numerical flux satisfies the *essentially three-point* consistency

$$H(\cdot, v, v, \cdot) = f(v). \tag{4.7}$$

2. *Numerical viscosity.* The second expression on the right of (4.2) accounts for the numerical viscosity of the scheme. Taylor's expansion shows that for smooth u's, this amount of numerical viscoity is of order $\sim(\Delta x)^3(a(u)u_{xxx})_x/8$. This $\mathcal{O}(\Delta x)^3$ term, uniformly bounded w.r.t. $1/\Delta t$, should be contrasted with the corresponding numerical viscosity terms of order $\mathcal{O}((\Delta x)^2/\Delta t)$ in the first-order LxF scheme (indicated earlier in (2.7)) and of order $\mathcal{O}((\Delta x)^4/\Delta t)$ in the second-order NT scheme.

3. *Simplicity.* We again would like to emphasize the simplicity of the second-order semi-discrete central scheme, (4.2), so that it does *not* require any information about the eigenstructure of the underlying problem beyond the CFL-related speeds, $a_{j+1/2}(t)$. The computation of the numerical derivatives, $(u_x)_j(t)$, is carried out *componentwise*; no specific knowledge of characteristic decomposition based on (approximate) Riemann solvers is required.

4. *First-order reduction.* If we reset all the numerical derivatives, $(u_x)_j(t) = 0$, then (4.2) is reduced to the first-order semi-discrete central scheme corresponding to the $\Delta t \downarrow 0$-limit of the Rusanov scheme, (3.10),

$$\frac{d}{dt}u_j(t) = -\frac{f(u_{j+1}(t)) - f(u_{j-1})}{2\Delta x} + \frac{1}{2\Delta x}\left[a_{j+1/2}(t)(u_{j+1}(t) - u_j(t)) - a_{j-1/2}(t)(u_j(t) - u_{j-1}(t))\right]. \tag{4.8}$$

We conclude this section with the proof of the one-dimensional scalar TVD property for our new semi-discrete scheme.

THEOREM 4.1 (TVD of Semi-discrete Central Scheme). *Consider the scalar semi-discrete central scheme* (4.2), *with intermediate values* $u^{\pm}_{j\pm1/2}$ *in* (4.5) *based on approximate derivatives* $(u_x)_j(t)$ *satisfying* (4.6), *e.g., the family of minmod-like limiters* (*with* $\theta = 1$ *corresponding to* (2.4))

$$(u_x)^n_j := \operatorname{minmod}\left(\theta\frac{u^n_j - u^n_{j-1}}{\Delta x}, \frac{u^n_{j+1} - u^n_{j-1}}{2\Delta x}, \theta\frac{u^n_{j+1} - u^n_j}{\Delta x}\right), \qquad 1 \le \theta \le 2. \quad (4.9)$$

Then the following TVD property holds:

$$\|u(\cdot,t)\|_{BV} := \sum_j |u_{j+1}(t) - u_j(t)| \le \|u(\cdot,0)\|_{BV}.$$

Remark. Notice that in the scalar case the local propagation speeds are given by

$$a_{j+1/2}(t) := \max_{u\in[u^-_{j+1/2}(t),u^+_{j+1/2}(t)]} |f'(u)|, \quad (4.10)$$

and in the special case of convex f, this is further simplified:

$$a_{j+1/2}(t) := \max\{|f'(u^-_{j+1/2}(t))|, |f'(u^+_{j+1/2}(t))|\}. \quad (4.11)$$

Proof. The second-order flux in (4.2), $H_{j+1/2}(t)$, can be viewed as a generalized MUSCL flux [40],

$$H_{j+1/2}(t) = H^{\text{Rus}}\left(u^+_{j+1/2}(t), u^-_{j+1/2}(t)\right),$$

expressed in terms of the first-order E-flux $H^{\text{Rus}} = H^{\text{Rus}}(u_\ell, u_r)$, associated with the first-order Rusanov scheme (4.8),

$$H^{\text{Rus}}(u_\ell, u_r) := \frac{f(u_\ell) + f(u_r)}{2} - \frac{a_{\ell r}}{2}(u_r - u_\ell), \qquad a_{\ell r} = \max_{u\in[u_\ell,u_r]} |f'(u)|.$$

According to [47], the TVD property of such scalar, semi-discrete generalized MUSCL schemes is guaranteed if (consult [47, Example 2.4])

$$\left|\frac{(u_x)_{j+1/2}}{\Delta u_{j\pm1/2}}\right| \le 2. \quad (4.12)$$

This is clearly fulfilled by the choice of approximate derivatives in (4.9). (We note in passing the necessity of the clipping phenomenon, (4.6), enforced by (4.12).) ■

4.2. *One-Dimensional Convection–Diffusion Equations*

Consider the convection–diffusion equation (1.2). If the dissipation flux, $Q(u, u_x)$, is a nonlinear function, then Eq. (1.2) can be a *strongly* degenerate parabolic equation which admits nonsmooth solutions. To solve it numerically is a highly challenging problem. In this context, the operator splitting technique was used in, e.g., [6, 8, 12, 20, 22, 23], yet this approach suffers the familiar limitations of splitting, e.g., limited accuracy, etc.

Our second-order semi-discrete scheme, (4.3)–(4.4), can be applied to Eq. (1.2) in a straightforward manner, since we can treat the hyperbolic and the parabolic parts of (1.2) simultaneously. This results in the following conservative scheme:

$$\dot{u}_j(t) = -\frac{H_{j+1/2}(t) - H_{j-1/2}(t)}{\Delta x} + \frac{P_{j+1/2}(t) - P_{j-1/2}(t)}{\Delta x}. \tag{4.13}$$

Here, $H_{j+1/2}(t)$ is our numerical convection flux, (4.4), and $P_{j+1/2}(t)$ is a reasonable approximation to the diffusion flux, e.g., the simplest central difference approximation

$$P_{j+1/2}(t) = \frac{1}{2}\left[Q\left(u_j(t), \frac{u_{j+1}(t) - u_j(t)}{\Delta x}\right) + Q\left(u_{j+1}(t), \frac{u_{j+1}(t) - u_j(t)}{\Delta x}\right)\right]. \tag{4.14}$$

4.3. *Multidimensional Extensions*

Our second-order semi-discrete schemes, (4.2) and (4.13), (4.4), (4.14), can be extended to both *multidimensional* hyperbolic and parabolic problems. Without loss of generality, let us consider the *two-dimensional* convection–diffusion equation

$$u_t + f(u)_x + g(u)_y = Q^x(u, u_x, u_y)_x + Q^y(u, u_x, u_y)_y, \tag{4.15}$$

where $Q^x \equiv Q^y \equiv 0$ corresponds to the two-dimensional hyperbolic conservation law.

We use a uniform spatial grid, $(x_j, y_k) = (j\Delta x, k\Delta y)$. Suppose that we have computed the solution at some time level t and have reconstructed the two-dimensional, non-oscillatory piecewise-linear polynomial approximation

$$u(x, y, t) \approx \sum_{j,k} [u_{j,k}(t) + (u_x)_{j,k}(t)(x - x_j) + (u_y)_{j,k}(t)(y - y_k)]\mathbf{1}_{[x_{j-1/2}, x_{j+1/2}] \times [y_{k-1/2}, y_{k+1/2}]}.$$

Here, $x_{j\pm1/2} := x_j \pm \frac{\Delta x}{2}$, $y_{k\pm1/2} := y_k \pm \frac{\Delta y}{2}$; $(u_x)_{j,k}(t)$ and $(u_y)_{j,k}(t)$ are numerical derivatives, which approximate the exact ones, $u_x(x_j, y_k, t)$ and $u_y(x_j, y_k, t)$, respectively. With a proper choice of numerical derivatives, the reconstruction of piecewise polynomial approximation is nonoscillatory. For example, using the minmod limiter, (2.4), guarantees the nonoscillatory property in the sense of satisfying a (local) scalar maximum principle; consult [18, Thm. 1].

The 2D extension of the scheme (4.13), (4.4), (4.14) can be written in the conservative form

$$\begin{aligned}\frac{d}{dt}u_{j,k}(t) = &-\frac{H^x_{j+1/2,k} - H^x_{j-1/2,k}}{\Delta x} - \frac{H^y_{j,k+1/2} - H^y_{j,k-1/2}}{\Delta y} \\ &+ \frac{P^x_{j+1/2,k} - P^x_{j-1/2,k}}{\Delta x} + \frac{P^y_{j,k+1/2} - P^y_{j,k-1/2}}{\Delta y}.\end{aligned} \tag{4.16}$$

Here, $H^x_{j+1/2,k} \equiv H^x_{j+1/2,k}(t)$ and $H^y_{j,k+1/2} \equiv H^y_{j,k+1/2}(t)$ are x- and y-numerical convection fluxes, respectively (viewed as a generalization of the one-dimensional flux constructed above in (4.4)),

$$H^x_{j+1/2,k}(t) := \frac{f\left(u^+_{j+1/2,k}(t)\right) + f\left(u^-_{j+1/2,k}(t)\right)}{2} - \frac{a^x_{j+1/2,k}(t)}{2}\left[u^+_{j+1/2,k}(t) - u^-_{j+1/2,k}(t)\right], \tag{4.17}$$

$$H^y_{j,k+1/2}(t) := \frac{g\left(u^+_{j,k+1/2}(t)\right) + g\left(u^-_{j,k+1/2}(t)\right)}{2} - \frac{a^y_{j,k+1/2}(t)}{2}\left[u^+_{j,k+1/2}(t) - u^-_{j,k+1/2}(t)\right],$$

which are expressed in terms of the intermediate values

$$\begin{aligned} u^{\pm}_{j+1/2,k}(t) &:= u_{j+1,k}(t) \mp \frac{\Delta x}{2}(u_x)_{j+1/2\pm 1/2,k}(t), \\ u^{\pm}_{j,k+1/2}(t) &:= u_{j,k+1}(t) \mp \frac{\Delta y}{2}(u_y)_{j,k+1/2\pm 1/2}(t), \end{aligned} \tag{4.18}$$

and the local speeds, $a^x_{j+1/2,k}(t)$ and $a^y_{j,k+1/2}(t)$, are computed, e.g., by

$$a^x_{j+1/2,k}(t) := \max_{\pm} \rho\left(\frac{\partial f}{\partial u}\left(u^{\pm}_{j+1/2,k}(t)\right)\right), \qquad a^y_{j,k+1/2}(t) := \max_{\pm} \rho\left(\frac{\partial g}{\partial u}\left(u^{\pm}_{j,k+1/2}(t)\right)\right). \tag{4.19}$$

Similarly, $P^x_{j+1/2,k} \equiv P^x_{j+1/2,k}(t)$ and $P^y_{j,k+1/2} \equiv P^y_{j,k+1/2}(t)$ are the corresponding x- and y-numerical diffusion fluxes, given by

$$\begin{aligned} P^x_{j+1/2,k} &:= \frac{1}{2}\left[Q^x\left(u_{j,k}, \frac{u_{j+1,k}-u_{j,k}}{\Delta x}, (u_y)_{j,k}\right) \right. \\ &\qquad \left. + Q^x\left(u_{j+1,k}, \frac{u_{j+1,k}-u_{j,k}}{\Delta x}, (u_y)_{j+1,k}\right)\right], \\ P^y_{j,k+1/2} &:= \frac{1}{2}\left[Q^y\left(u_{j,k}, (u_x)_{j,k}, \frac{u_{j,k+1}-u_{j,k}}{\Delta y}\right) \right. \\ &\qquad \left. + Q^y\left(u_{j,k+1}, (u_x)_{j,k+1}, \frac{u_{j,k+1}-u_{j,k}}{\Delta y}\right)\right]. \end{aligned} \tag{4.20}$$

5. FROM SEMI-DISCRETE BACK TO FULLY DISCRETE—THE GENERAL SETUP

The two-dimensional semi-discrete central scheme (4.2) forms a system of nonlinear ODEs, the so-called "method of lines" for the discrete unknowns $\{u_{j,k}(t)\}$. To integrate in time, one must introduce a variable time step, Δt^n, stepping forward from time level t^n to $t^{n+1} := t^n + \Delta t^n$. We start by considering the simplest scenario of first-order time differencing. The nonoscillatory behavior of the forward Euler scheme is summarized in the maximum principle stated in Theorem 5.1 below. To retain the overall high accuracy of the spatial differencing, however, higher-order stable time discretizations are required. To this end, the forward Euler time differencing can be used as a building block for higher-order Runge–Kutta and multi-level ODE solvers. In particular, second- and third-order ODE solvers can be constructed by *convex combinations* of the simple forward Euler differencing, retaining the overall maximum principle. Thus, we conclude in Corollaries 5.1 and 5.2 below with a fully discrete second-order central scheme satisfying the two-dimensional scalar maximum principle.

We begin with

THEOREM 5.1 (Maximum Principle). *Consider the two-dimensional central scheme*

$$u^{n+1}_{j,k} = u^n_{j,k} - \frac{\Delta t^n}{\Delta x}\left(H^x_{j+1/2,k}(t^n) - H^x_{j-1/2,k}(t^n)\right) - \frac{\Delta t^n}{\Delta y}\left(H^y_{j,k+1/2}(t^n) - H^y_{j,k-1/2}(t^n)\right). \tag{5.1}$$

Here, $H^x(t)$ and $H^y(t)$ are the numerical fluxes given in (4.17)–(4.19); *let their numerical derivatives be determined by one of the following one-parameter family of minmod-like*

limiters:

$$(u_x)^n_{j,k} := \operatorname{minmod}\left(\theta\frac{u^n_{j,k}-u^n_{j-1,k}}{\Delta x}, \frac{u^n_{j+1,k}-u^n_{j-1,k}}{2\Delta x}, \theta\frac{u^n_{j+1,k}-u^n_{j,k}}{\Delta x}\right), \qquad 1\le\theta\le 2,$$
$$(u_y)^n_{j,k} := \operatorname{minmod}\left(\theta\frac{u^n_{j,k}-u^n_{j,k-1}}{\Delta y}, \frac{u_{j,k+1}-u_{j,k-1}}{2\Delta y}, \theta\frac{u^n_{j,k+1}-u^n_{j,k}}{\Delta y}\right), \qquad 1\le\theta\le 2. \tag{5.2}$$

Assume the following CFL condition holds:

$$\max\left(\frac{\Delta t^n}{\Delta x}\max_u|f'(u)|, \frac{\Delta t^n}{\Delta y}\max_u|g'(u)|\right)\le\frac{1}{8}. \tag{5.3}$$

Then the resulting fully discrete central scheme satisfies the maximum principle

$$\max_{j,k}\{u_{j,k}(t^{n+1})\}\le\max_{j,k}\{u_{j,k}(t^n)\}. \tag{5.4}$$

Proof. With $\lambda^n := \Delta t^n/\Delta x$ and $\mu^n := \Delta t^n/\Delta y$ denoting the x- and y-mesh ratios, the forward Euler time discretization of our scheme takes the explicit form

$$\begin{aligned}u^{n+1}_{j,k} = u^n_{j,k} &- \frac{\lambda^n}{2}\big[f\big(u^+_{j+1/2,k}(t^n)\big)+f\big(u^-_{j+1/2,k}(t^n)\big)-f\big(u^+_{j-1/2,k}(t^n)\big)-f\big(u^-_{j-1/2,k}(t^n)\big)\\
&-a^x_{j+1/2,k}(t^n)\big\{u^+_{j+1/2,k}(t^n)-u^-_{j+1/2,k}(t^n)\big\}+a^x_{j-1/2,k}(t^n)\big\{u^+_{j-1/2,k}(t^n)\\
&-u^-_{j-1/2,k}(t^n)\big\}\big]-\frac{\mu^n}{2}\big[g\big(u^+_{j,k+1/2}(t^n)\big)+g\big(u^-_{j,k+1/2}(t^n)\big)-g\big(u^+_{j,k-1/2}(t^n)\big)\\
&-g\big(u^-_{j,k-1/2}(t^n)\big)-a^y_{j,k+1/2}(t^n)\big\{u^+_{j,k+1/2}(t^n)-u^-_{j,k+1/2}(t^n)\big\}\\
&+a^y_{j,k-1/2}(t^n)\big\{u^+_{j,k-1/2}(t^n)-u^-_{j,k-1/2}(t^n)\big\}\big].\end{aligned}$$

To simplify notations, we use the standard abbreviations

$$\Delta^x_{j\pm1/2,k}u := u^+_{j\pm1/2,k}(t^n)-u^-_{j\pm1/2,k}(t^n), \qquad \Delta^x_{j,k}f := f\big(u^-_{j+1/2,k}(t^n)\big)-f\big(u^+_{j-1/2,k}(t^n)\big),$$

with the similar notations for y-differences, e.g., $\Delta^y_{j,k}g := g(u^-_{j,k+1/2}(t^n))-g(u^+_{j,k-1/2}(t^n))$, etc. Then our scheme can be rewritten as follows (where all the quantities on the right are taken at time level $t=t^n$):

$$\begin{aligned}u^{n+1}_{j,k} = \frac{u^-_{j+1/2,k}+u^+_{j-1/2,k}+u^-_{j,k+1/2}+u^+_{j,k-1/2}}{4} &- \frac{\lambda^n}{2}\left[\frac{\Delta^x_{j+1/2,k}f}{\Delta^x_{j+1/2,k}u}\big(u^+_{j+1/2,k}-u^-_{j+1/2,k}\big)\right.\\
&+2\frac{\Delta^x_{j,k}f}{\Delta^x_{j,k}u}\big(u^-_{j+1/2,k}-u^+_{j-1/2,k}\big)+\frac{\Delta^x_{j-1/2,k}f}{\Delta^x_{j-1/2,k}u}\big(u^+_{j-1/2,k}-u^-_{j-1/2,k}\big)\\
&\left.-a^x_{j+1/2,k}\big(u^+_{j+1/2,k}-u^-_{j+1/2,k}\big)+a^x_{j-1/2,k}\big(u^+_{j-1/2,k}-u^-_{j-1/2,k}\big)\right]\\
&-\frac{\mu^n}{2}\left[\frac{\Delta^y_{j,k+1/2}g}{\Delta^y_{j,k+1/2}u}\big(u^+_{j,k+1/2}-u^-_{j,k+1/2}\big)+2\frac{\Delta^y_{j,k}g}{\Delta^y_{j,k}u}\big(u^-_{j,k+1/2}-u^+_{j,k-1/2}\big)\right.\\
&+\frac{\Delta^y_{j,k-1/2}g}{\Delta^y_{j,k-1/2}u}\big(u^+_{j,k-1/2}-u^-_{j,k-1/2}\big)-a^y_{j,k+1/2}\big(u^+_{j,k+1/2}-u^-_{j,k+1/2}\big)\\
&\left.+a^y_{j,k-1/2}\big(u^+_{j,k-1/2}-u^-_{j,k-1/2}\big)\right].\end{aligned}$$

Rearranging the terms, we find that $u^{n+1}_{j,k}$ is given by the following linear combination of the intermediate values, $u^{\pm}_{j\pm1/2,k}$ and $u^{\pm}_{j,k\pm1/2}$:

$$\begin{aligned}
u^{n+1}_{j,k} = {} & \frac{\lambda^n}{2}\left\{a^x_{j+1/2,k} - \frac{\Delta^x_{j+1/2,k} f}{\Delta^x_{j+1/2,k} u}\right\} u^+_{j+1/2,k} + \frac{\lambda^n}{2}\left\{a^x_{j-1/2,k} + \frac{\Delta^x_{j-1/2,k} f}{\Delta^x_{j-1/2,k} u}\right\} u^-_{j-1/2,k} \\
& + \left\{\frac{1}{4} + \frac{\lambda^n}{2}\left[\frac{\Delta^x_{j+1/2,k} f}{\Delta^x_{j+1/2,k} u} - a^x_{j+1/2,k} - 2\frac{\Delta^x_{j,k} f}{\Delta^x_{j,k} u}\right]\right\} u^-_{j+1/2,k} \\
& + \left\{\frac{1}{4} - \frac{\lambda^n}{2}\left[\frac{\Delta^x_{j+1/2,k} f}{\Delta^x_{j+1/2,k} u} + a^x_{j-1/2,k} - 2\frac{\Delta^x_{j,k} f}{\Delta^x_{j,k} u}\right]\right\} u^+_{j-1/2,k} \\
& + \frac{\mu^n}{2}\left\{a^y_{j,k+1/2} - \frac{\Delta^y_{j,k+1/2} g}{\Delta^y_{j,k+1/2} u}\right\} u^+_{j,k+1/2} + \frac{\mu^n}{2}\left\{a^y_{j,k-1/2} + \frac{\Delta^y_{j,k-1/2} g}{\Delta^y_{j,k-1/2} u}\right\} u^-_{j,k-1/2} \\
& + \left\{\frac{1}{4} + \frac{\mu^n}{2}\left[\frac{\Delta^y_{j,k+1/2} g}{\Delta^y_{j,k+1/2} u} - a^y_{j,k+1/2} - 2\frac{\Delta^y_{j,k} g}{\Delta^y_{j,k} u}\right]\right\} u^-_{j,k+1/2} \\
& + \left\{\frac{1}{4} - \frac{\mu^n}{2}\left[\frac{\Delta^y_{j,k-1/2} g}{\Delta^y_{j,k-1/2} u} + a^y_{j,k-1/2} - 2\frac{\Delta^y_{j,k} g}{\Delta^y_{j,k} u}\right]\right\} u^+_{j,k-1/2}. \qquad (5.5)
\end{aligned}$$

Note that all the coefficients in (5.5) are positive due to our CFL assumption, (5.3). This means that the linear combination on the RHS of (5.5) is a *convex* combination and hence the value of $u^{n+1}_{j,k}$ does not exceed the values of $u^{\pm}_{j\pm1/2,k}$ and $u^{\pm}_{j,k\pm1/2}$. And since our choice of minmod-like approximate derivatives in (5.2) guarantees that these intermediate values, $u^{\pm}$, satisfy a local maximum principle w.r.t. the original averages, u^n, e.g., [18], $\max_{j,k}\{u^{\pm}_{j\pm1/2,k}(t), u^{\pm}_{j,k\pm1/2}(t)\} \le \max_{j,k}\{u_{j,k}(t)\}$, the result (5.4) then follows. ■

The forward Euler scheme is limited to first-order accuracy. It can be used, however, as a building block for higher-order schemes based on Runge–Kutta (RK) or multi-level time differencing. Shu and Osher [44, 45] have identified a whole family of such schemes, based on *convex* combinations of forward Euler steps.

To this end, we let $C[w]$ denote our spatial recipe (4.17)–(4.19) for central differencing a grid function $w = \{w_{j,k}\}$,

$$C[w] := -\left[\frac{H^x_{j+1/2,k}(w) - H^x_{j-1/2,k}(w)}{\Delta x} + \frac{H^y_{j,k+1/2}(w) - H^y_{j,k-1/2}(w)}{\Delta y}\right]. \qquad (5.6)$$

Expressed in terms of the forward Euler solver, $w + \Delta t C[w]$, we consider the one-parameter family of RK schemes

$$\begin{aligned}
u^{(1)} &= u^n + \Delta t^n C[u^n] \\
u^{(\ell+1)} &= \eta_\ell u^n + (1-\eta_\ell)\big(u^{(\ell)} + \Delta t^n C\big[u^{(\ell)}\big]\big), \qquad \ell = 1, 2, \ldots, s-1, \qquad (5.7) \\
u^{n+1} &:= u^{(s)}.
\end{aligned}$$

In Table 5.1 we quote the preferred second- and third-order choices of [45]. We state

COROLLARY 5.1 (Maximum Principle for Runge–Kutta Time Differencing). *Assume that the CFL condition* (5.3) *holds. Then the fully discrete central scheme* (4.17)–(4.19), (5.2), (5.7) *with* η_m *specified in Table* 5.1 *satisfies the maximum principle* (5.4).

TABLE 5.1
Runge–Kutta Methods

	η_1	η_2
Second order time differencing		
Two-step modified Euler ($s=2$)	$\frac{1}{2}$	—
Third order time differencing		
Three-step method ($s=3$)	$\frac{3}{4}$	$\frac{1}{3}$

A similar two-parameter family of *multi-level* methods was identified in [44]. They take the particularly simple form

$$u^{n+1} = \eta(u^n + c_0\Delta t^n C[u^n]) + (1-\eta)(u^{n-s} + c_s\Delta t^n C[u^{n-s}]), \tag{5.8}$$

with positive coefficients given in Table 5.2. We state

COROLLARY 5.2 (Maximum Principle for Multi-level Time Differencing). *Assume that the CFL condition*

$$\max\left(\frac{\Delta t^n}{\Delta x}\max_u|f'(u)|, \frac{\Delta t^n}{\Delta y}\max_u|g'(u)|\right) \le \min_{c_k}\frac{1}{8c_k} \tag{5.9}$$

holds. Then the fully discrete multi-level central scheme (4.17)–(4.19), (5.2), (5.8), *with* η *and* c*'s specified in Table* 5.2, *satisfies the maximum principle* (5.4).

We close by noting that Corollaries 5.1 and 5.2 extend the maximum principle for the second-order fully discrete two-dimensional scheme introduced in [18, Thm. 1].

6. NUMERICAL EXAMPLES

We conclude this paper with a number of numerical examples. In all the numerical results presented below we have used the θ-dependent family of limiters corresponding to (4.9). (These are in general the less dissipative limiter than the original minmod, (2.4), corresponding to (4.9) with $\theta=1$). The spatial derivative of $u(x,t)$ is approximated by

$$u_x(x,t) \approx \text{minmod}\left(\theta\frac{\bar u(x+a)-\bar u(x)}{a}, \frac{\bar u(x+a)-\bar u(x-b)}{a+b}, \theta\frac{\bar u(x)-\bar u(x-b)}{b}\right), \tag{6.1}$$

TABLE 5.2
Multi-level Methods

	η	c_0	c_s
Second-order time differencing			
4-level method ($s=2$)	$\frac{3}{4}$	2	0
5-level method ($s=3$)	$\frac{8}{9}$	$\frac{3}{2}$	0
Third-order time differencing			
5-level method ($s=3$)	$\frac{16}{27}$	3	$\frac{12}{11}$
6-level method ($s=4$)	$\frac{25}{32}$	2	$\frac{10}{7}$
7-level method ($s=5$)	$\frac{108}{125}$	$\frac{5}{3}$	$\frac{30}{17}$

where a and b are appropriate grid scales, and the multivariable minmod function is defined by

$$\text{minmod}(x_1, x_2, \ldots) = \begin{cases} \min_j\{x_j\}, & \text{if } x_j > 0 \ \ \forall j, \\ \max_j\{x_j\}, & \text{if } x_j < 0 \ \ \forall j, \\ 0, & \text{otherwise.} \end{cases}$$

The parameter $\theta \in [1, 2]$ has been chosen in the optimal way in every example. Note that $\theta = 2$ corresponds to the least dissipative limiter (no new local extrema are introduced), whereas $\theta = 1$ ensures a nonoscillatory nature of the approximate solution in the sense that there is no increase of the total-variation. The reconstruction depicted in Fig. 3.2, for example, does not increase in the variation at the interface $x_{j-1/2}$ but it is an oscillatory one since new extrema is introduced at $x_{j+1/2}$. In the scalar examples below, $\theta = 2$ has provided a satisfactory results, but consult the nonconvex Buckley–Levertt equation in Fig. 6.7 as a counterexample; for systems the optimal values of θ vary between 1.1 and 1.5.

Another point we would like to stress concerns the time discretization of our semi-discrete central schemes. In general, the Runge–Kutta time differencing is preferable over the multi-level differencing, since the former enables a straightforward use of variable time steps. We note that for the standard explicit RK methods the time step can be very small due to their strict stability restriction. There are two different approaches to increasing efficiency at this point. First, one can use implicit or explicit–implicit ODE solvers. These methods are unconditionally stable, but they require inverting nonlinear operators (in the general case of a nonlinear diffusion), which is a computationally expensive and analytically complicated procedure.

In all the numerical examples shown below, we preferred the second approach—to solve systems of ODEs by means of the explicit embedded integration third-order RK method recently introduced by Medovikov [37] (his original code, DUMKA3, was used). This high-order differencing produces accurate results, and its larger stability domains (in comparison with the standard RK methods) allow us to use larger time steps; the explicit form retains simplicity, and the embedded formulas permit an efficient stepsize control. In practice these methods preserve all the advantages of explicit methods and work as fast as implicit methods (see [37] for details).

Remark. Below, we abbreviate by FD1 and SD1 the Rusanov first-order fully and semi-discrete schemes. We also use FD2 and SD2 notation for our second-order fully and semi-discrete schemes. As previously, LxF and NT stand for the Lax–Friedrichs and the Nessyahu–Tadmor schemes.

6.1. *One-Dimensional Scalar Linear Hyperbolic Equation*

EXAMPLE 1 (Linear Steady Shocks). First, consider the *simplest linear* equation with the zero flux, $f(u) = 0$,

$$u_t = 0, \tag{6.2}$$

subject to the discontinuous initial data,

$$u(x, 0) = \begin{cases} 1, & -0.5 < x < 0.5, \\ 0, & \text{otherwise.} \end{cases} \tag{6.3}$$

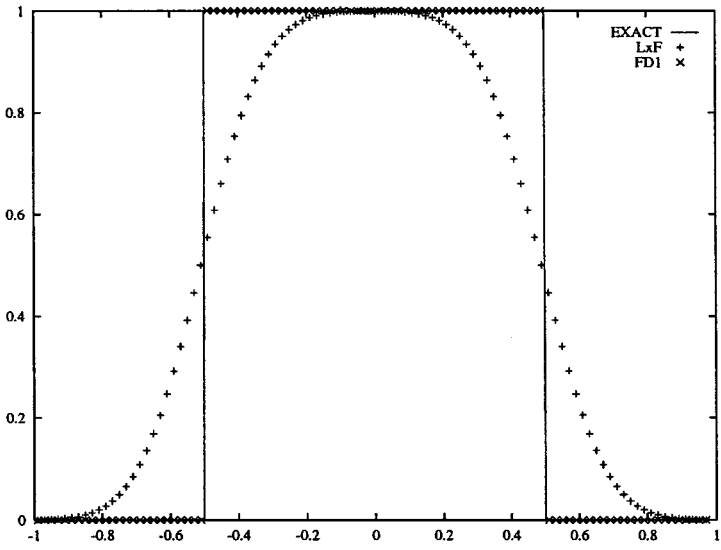

FIG. 6.3. Problem (6.2)–(6.3). $N = 100$, $T = 2$; first-order methods.

Notice that due to their *dissipative* nature, neither the LxF scheme nor the NT scheme provides a reasonable approximation to this problem. But using the Rusanov scheme and our second-order fully discrete scheme, which are, in some sense, the least dissipative central schemes, we achieve the perfect resolution of the discontinuities (the same result is obtained by the corresponding semi-discrete schemes).

In Figs. 6.3 and 6.4 the solutions computed by our schemes are compared with the (staggered) LxF and NT schemes. It also can be easily checked analytically that both the FD1 scheme and the FD2 schemes solve problem (6.2)–(6.3) exactly.

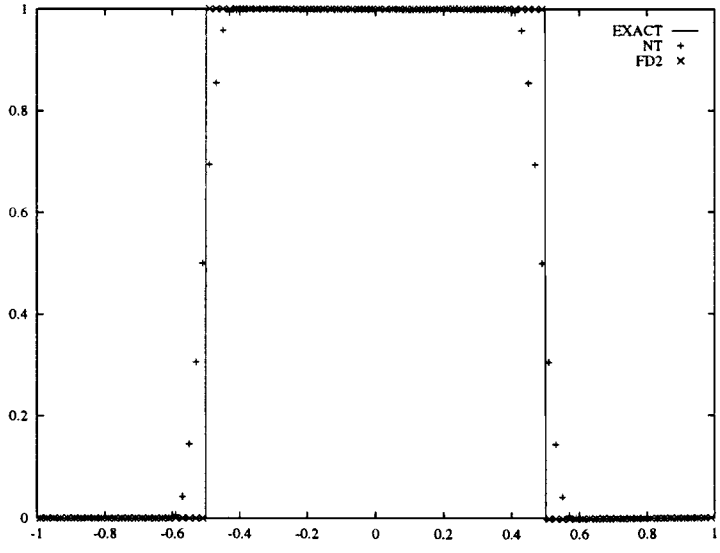

FIG. 6.4. Problem (6.2)–(6.3). $N = 100$, $T = 2$; second-order methods.

TABLE 6.1
Initial Value Problem (6.4), L^1- and L^∞-Norms of the Errors

	L^1-error				L^∞-error			
N	NT	Rate	FD2	Rate	NT	Rate	FD2	Rate
40	2.920e-03	—	8.716e-03	—	3.151e-03	—	7.818e-03	—
80	4.583e-04	2.67	1.876e-03	2.22	9.963e-04	1.66	2.598e-03	1.59
160	1.115e-04	2.04	3.892e-04	2.27	3.704e-04	1.43	9.262e-04	1.49
320	2.360e-05	2.24	7.943e-05	2.29	1.263e-04	1.55	2.881e-04	1.68
640	5.273e-06	2.16	1.659e-05	2.26	4.463e-05	1.50	1.028e-04	1.49
1280	1.249e-06	2.08	3.430e-06	2.27	1.690e-05	1.40	3.593e-05	1.52

EXAMPLE 2 (Accuracy Test). Let us consider the *linear* equation subject to periodic initial data

$$u_t + u_x = 0, \qquad u(x, 0) = \sin x. \tag{6.4}$$

This problem admits the global smooth solution that was computed at time $T = 1$ with the varying number of grid points, N.

In Table 6.1 we compare the accuracy of our second-order fully discrete scheme, FD2, with the accuracy of the NT scheme. These results show that for the FD2 scheme the absolute error is larger, but the rate of convergence is slightly higher than for the NT scheme.

6.2. *One-Dimensional Scalar Hyperbolic Conservation Laws*

EXAMPLE 3 (Burgers' Equation: Pre- and Post-shock Solutions). In this example we approximate solutions to the inviscid Burgers' equation,

$$u_t + \left(\frac{u^2}{2}\right)_x = 0. \tag{6.5}$$

Let us start with the case of smooth periodic initial data, e.g.,

$$u(x, 0) = 0.5 + \sin x. \tag{6.6}$$

The well-known solution of (6.5)–(6.6) develops a shock discontinuity at the critical time $T_c = 1$. Table 6.2 shows the L^1- and L^∞-norms of the errors at the pre-shock time $T = 0.5$

TABLE 6.2
Initial Value Problem (6.5)–(6.6), L^1- and L^∞-Norms of the Errors at $T = 0.5$

	L^1-error				L^∞-error			
N	NT	Rate	FD2	Rate	NT	Rate	FD2	Rate
40	1.011e-02	—	9.101e-03	—	6.782e-03	—	6.283e-03	—
80	2.116e-03	2.26	1.843e-03	2.30	2.951e-03	1.20	2.333e-03	1.43
160	4.705e-04	2.17	4.272e-04	2.11	9.918e-04	1.57	7.481e-04	1.64
320	1.095e-04	2.10	9.334e-05	2.19	3.727e-04	1.41	2.603e-04	1.52
640	2.517e-05	2.12	2.163e-05	2.11	1.248e-04	1.58	9.508e-05	1.45
1280	5.926e-06	2.09	4.867e-06	2.15	4.433e-05	1.49	3.132e-05	1.60

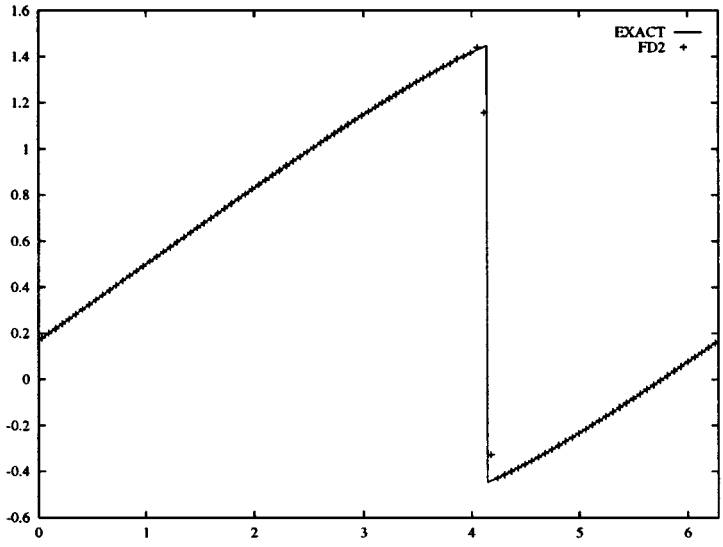

FIG. 6.5. Problem (6.5)–(6.6). $N = 100$, $T = 2$; the FD2 scheme.

when the solution is still infinitely smooth. Unlike the linear case (Example 2), both the absolute errors and the convergence rates of the FD2 scheme are better than the corresponding errors and rates of the NT scheme. This indicates a certain advantage of our fully discrete second-order scheme over the NT scheme while applied to nonlinear problems.

In Figs. 6.5 and 6.6 we present the approximate solutions at the post-shock time $T = 2$, when the shock is well developed. Second-order behavior is confirmed by the measuring Lip´-errors, [39], which are recorded in Table 6.3. Again, the solution obtained by the FD2 scheme is slightly more accurate than the solution computed by the NT scheme.

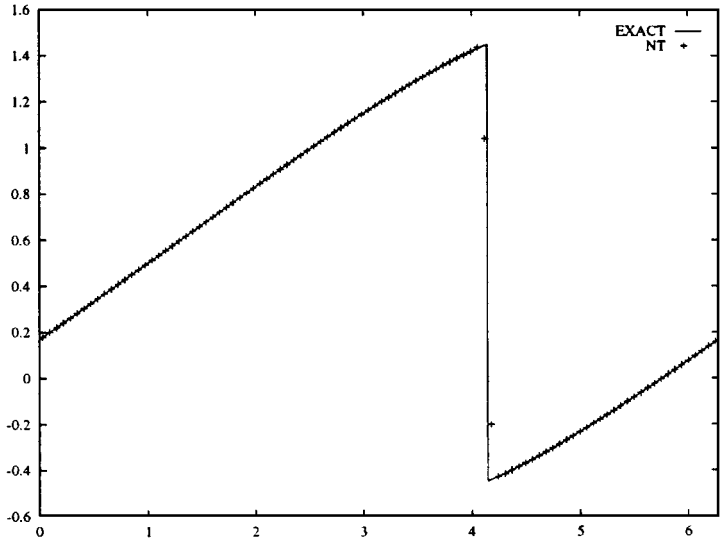

FIG. 6.6. Problem (6.5)–(6.6). $N = 100$, $T = 2$; the NT scheme.

TABLE 6.3
Initial Value Problem (6.5)–(6.6), Lip′-Norm of the Errors at $T = 2$

N	NT	Rate	FD2	Rate
40	1.233e-02	—	7.779e-03	—
80	1.904e-03	2.70	1.982e-03	1.97
160	4.809e-04	1.99	4.905e-04	2.01
320	1.253e-04	1.94	1.222e-04	2.01
640	3.415e-05	1.88	3.047e-05	2.00
1280	1.000e-05	1.77	7.558e-06	2.01

EXAMPLE 4 (Nonconvex Flux). In this example we show results of applying our fully discrete second-order scheme to the following Riemann problem:

$$u_t + \left[\frac{(u^2-1)(u^2-4)}{4}\right]_x = 0, \qquad u(x,0) = \begin{cases} 2, & \text{if } x < 0, \\ -2, & \text{if } x > 0. \end{cases} \tag{6.7}$$

The solutions to this initial value problem are depicted at time $T = 1.2$. Figure 6.7 demonstrates the clear advantage of our new FD2 scheme over the NT scheme; in particular, the latter seems to give a wrong solution (even after the grid refinement.[3] We note, however, that when a more restrictive minmod limiter was used (corresponding to $\theta = 1$ in (6.1)), the NT solution did converge to the entropy solution at the expense of additional smoothing on the edges of the Riemann fan, which can be noticed in Fig. 6.8.

6.3. *One-Dimensional Systems of Hyperbolic Conservation Laws*

EXAMPLE 5 (Euler Equations of Gas Dynamics). Let us consider the one-dimensional Euler System

$$\frac{\partial}{\partial t}\begin{bmatrix} \rho \\ m \\ E \end{bmatrix} + \frac{\partial}{\partial x}\begin{bmatrix} m \\ \rho u^2 + p \\ u(E+p) \end{bmatrix} = 0, \qquad p = (\gamma - 1)\cdot\left(E - \frac{\rho}{2}u^2\right),$$

where $\rho, u, m = \rho u$, p, and E are the density, velocity, momentum, pressure, and total energy, respectively. Here, the conserved quantities are $\vec{u} = (\rho, m, E)^T$, and the flux vector function is $f(\vec{u}) = (m, \rho u^2 + p, u(E+p))^T$. We solve this system subject to Riemann initial data,

$$\vec{u}(x,0) = \begin{cases} \vec{u}_L, & x < 0, \\ \vec{u}_R, & x > 0. \end{cases}$$

We apply our scalar-designed schemes to this problem in a straightforward manner. We now prefer the alternative approximation to the flux derivatives, needed in (3.6). The minmod limiter, (6.1), is employed directly on the corresponding values of $f(\vec{u})$ to avoid an expensive computation of the Jacobian, $\frac{\partial f}{\partial u}$.

[3] A similar failure of convergence towards the entropy solution by upwind approximation of nonconvex equations was reported in [5].

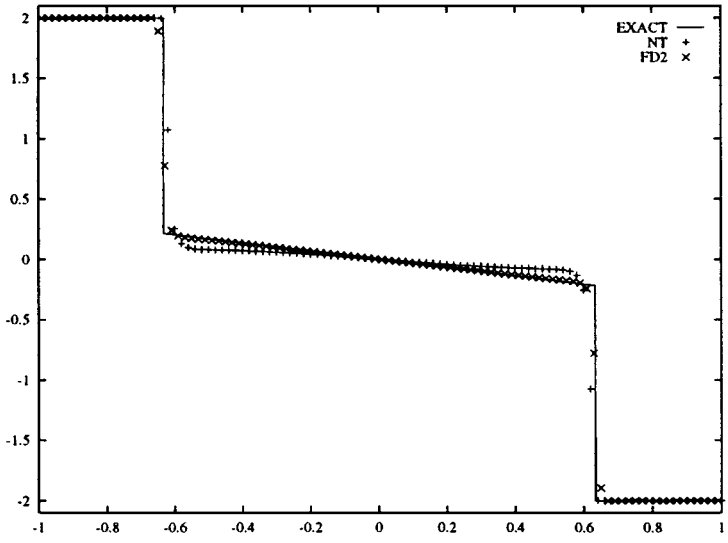

FIG. 6.7. Riemann IVP (6.7). $N = 100$.

We compute the solution to two different Riemann problems:

- The first Riemann problem was proposed by Sod [46]. The initial data are given by

$$\vec{u}_L = (1, 0, 2.5)^T, \qquad \vec{u}_R = (0.125, 0, 0.25)^T.$$

The approximations to the density, velocity, and pressure obtained by the FD2 scheme are presented in Figs. 6.9–6.14.

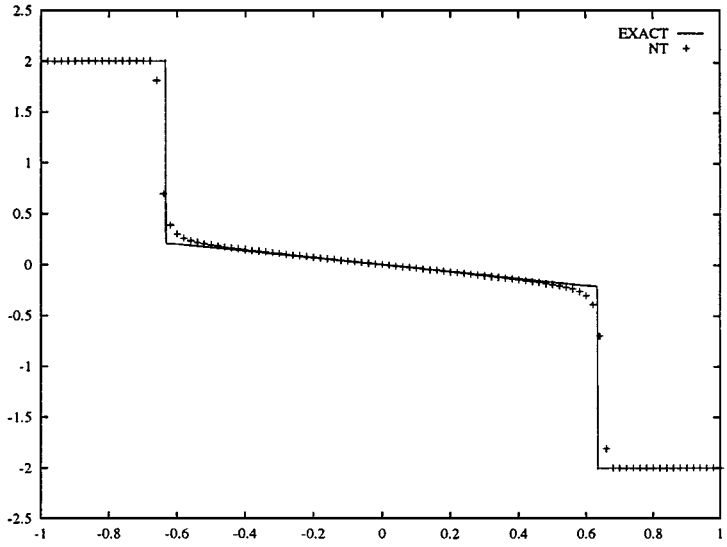

FIG. 6.8. Riemann IVP (6.7). $N = 100$.

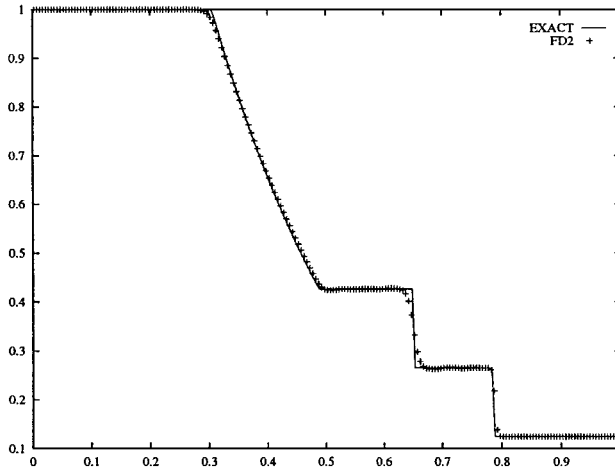

FIG. 6.9. Sod problem—density. $N = 200$, $T = 0.1644$.

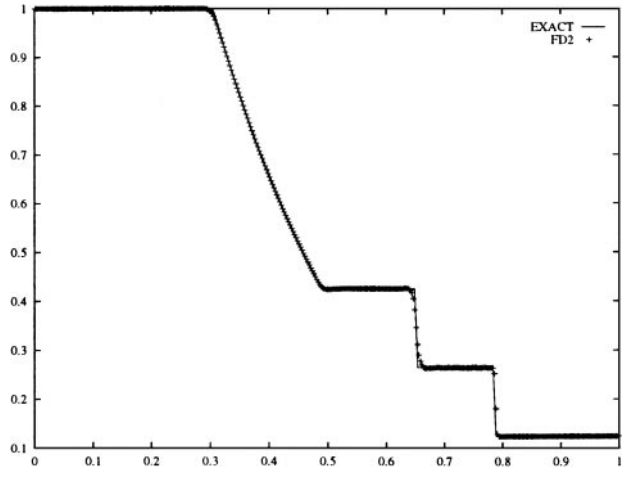

FIG. 6.10. Sod problem—density. $N = 400$, $T = 0.1644$.

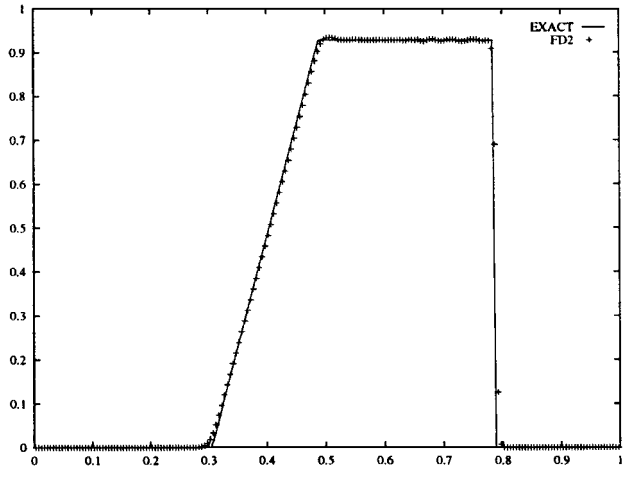

FIG. 6.11. Sod problem—velocity. $N = 200$, $T = 0.1644$.

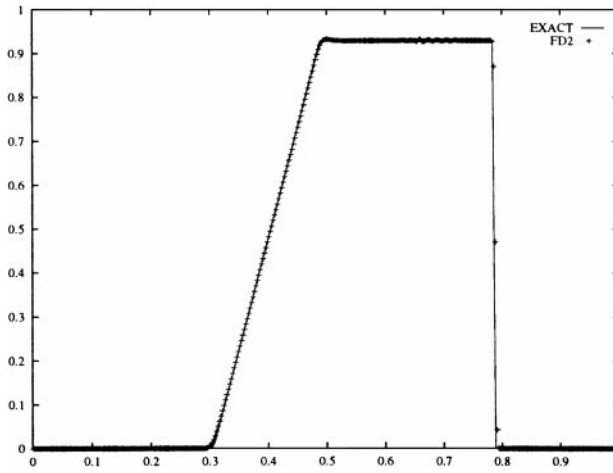

FIG. 6.12. Sod problem—velocity. $N = 400$, $T = 0.1644$.

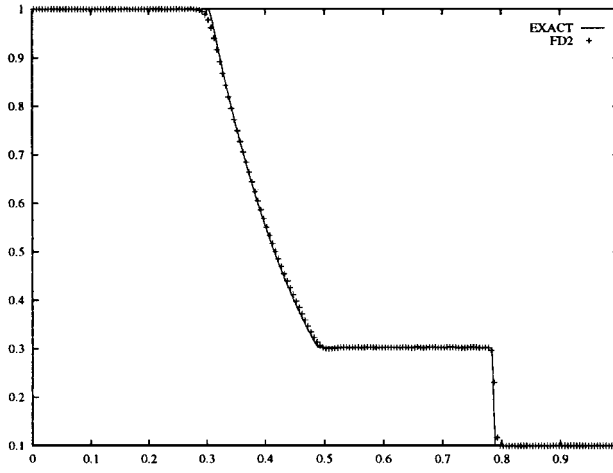

FIG. 6.13. Sod problem—pressure. $N = 200$, $T = 0.1644$.

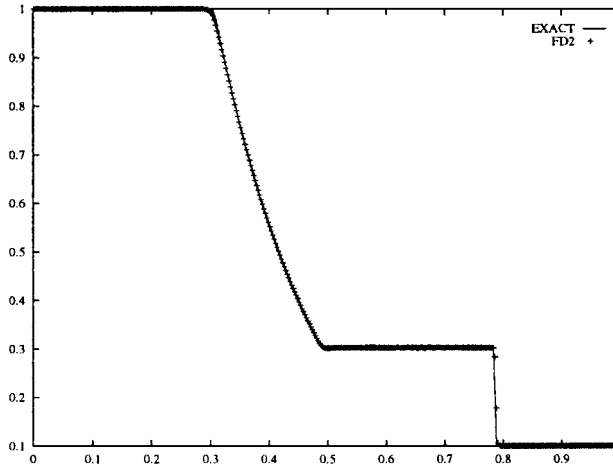

FIG. 6.14. Sod problem—pressure. $N = 400$, $T = 0.1644$.

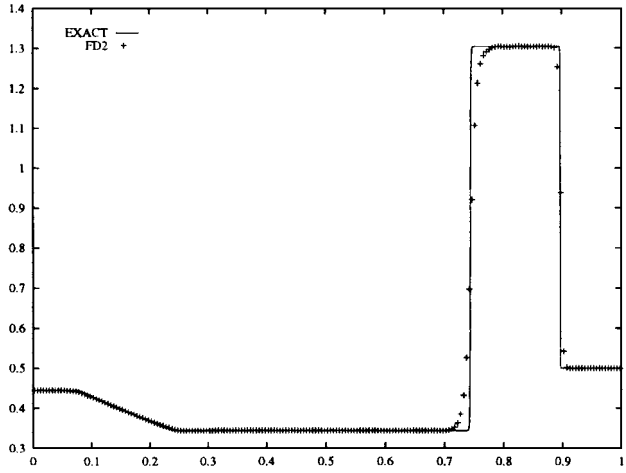

FIG. 6.15. Lax problem—density. $N = 200$, $T = 0.16$.

• The second Riemann problem was proposed by Lax [29]. The initial values are given by

$$\vec{u}_L = (0.445, 0.311, 8.928)^T, \qquad \vec{u}_R = (0.5, 0, 1.4275)^T.$$

The results computed by the FD2 scheme are shown in Figs. 6.15–6.20.

Our numerical results for this system are comparable with the results obtained in [38]. We would like to stress again that as in the case of the original NT scheme the characteristic decomposition is not required; i.e., our new schemes still can be applied componentwise.

Remark. In all the above 1D hyperbolic examples we have presented the numerical results obtained by our fully discrete scheme. We also tested the corresponding

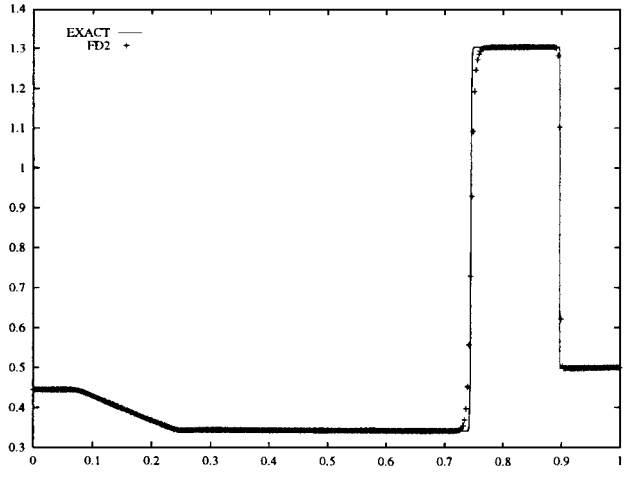

FIG. 6.16. Lax problem—density. $N = 400$, $T = 0.16$.

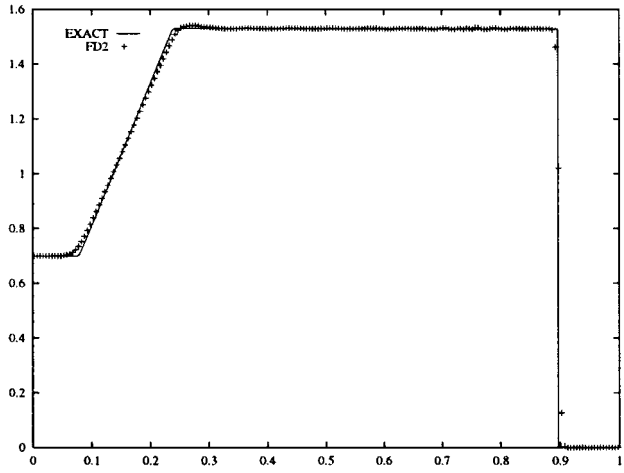

FIG. 6.17. Lax problem—velocity. $N = 200$, $T = 0.16$.

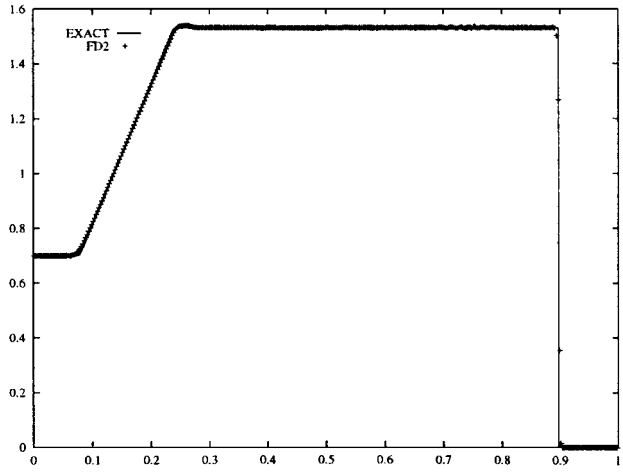

FIG. 6.18. Lax problem—velocity. $N = 400$, $T = 0.16$.

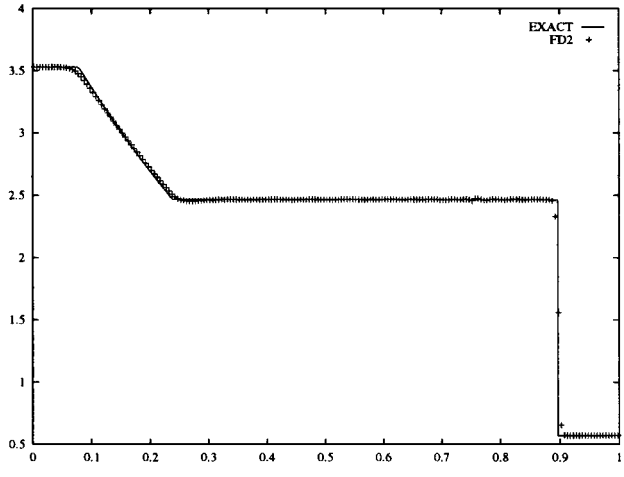

FIG. 6.19. Lax problem—pressure. $N = 200$, $T = 0.16$.

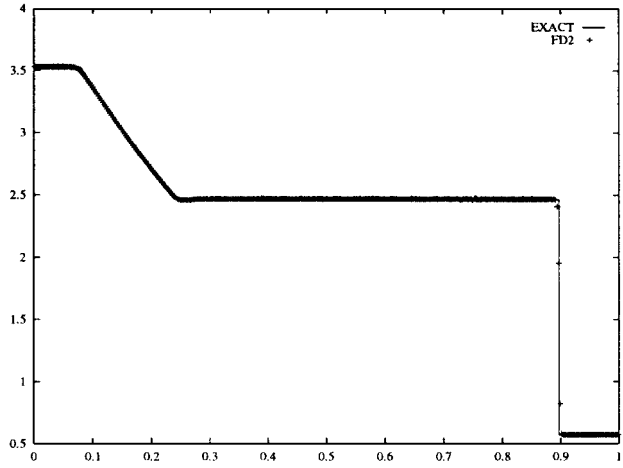

FIG. 6.20. Lax problem—pressure. $N = 400$, $T = 0.16$.

semi-discrete scheme on the same examples. The results are very similar, but the semi-discrete scheme is slightly more dissipative than the fully discrete one.

As we have already mentioned, the main advantage of the semi-discrete approach can be seen while we apply our scheme to (degenerate) parabolic convection–diffusion equations. Below, we show several examples of such problems.

6.4. *One-Dimensional Convection–Diffusion Equations*

EXAMPLE 6 (Burgers-Type Equation with Saturating Dissipation). We begin with the convection–diffusion equation with bounded dissipation flux proposed in [28]. Consider Eq. (1.3) with $f(u) = u^2$ subject to the Riemann initial data,

$$u(x, 0) = \begin{cases} 1.2, & x < 0, \\ -1.2, & x > 0. \end{cases} \tag{6.8}$$

It was proved in [12] that the solution to this initial value problem contains a subshock located at $x = 0$. This is why solving (1.3), (6.8) numerically is quite challenging problem.

Our second-order semi-discrete scheme, SD2, provides a very good resolution of the discontinuity (Fig. 6.21) while the fully discrete NT scheme fails to resolve it (Fig. 6.22; see also numerical results in [28]). The SD2 scheme was tested on all the examples from [12]. The numerical results are highly satisfactory, and using this semi-discrete approach no operator splitting is needed (consult [12] for details).

EXAMPLE 7 (Buckley–Leverett Equation). Next, let us consider the scalar convection–diffusion Buckley–Leverett equation (1.2) with $Q(u, s) = \nu(u)s$,

$$u_t + f(u)_x = \varepsilon(\nu(u)u_x)_x, \qquad \varepsilon\nu(u) \geq 0. \tag{6.9}$$

This is a prototype model for oil reservoir simulations (two-phase flow). Typically, $\nu(u)$ vanishes at some values of u, and (6.9) is a degenerate parabolic equation. Usually, the operator splitting technique is used (see [6, 8, 20, 22, 23]) to solve it numerically, but the limitations of such an approach are well known.

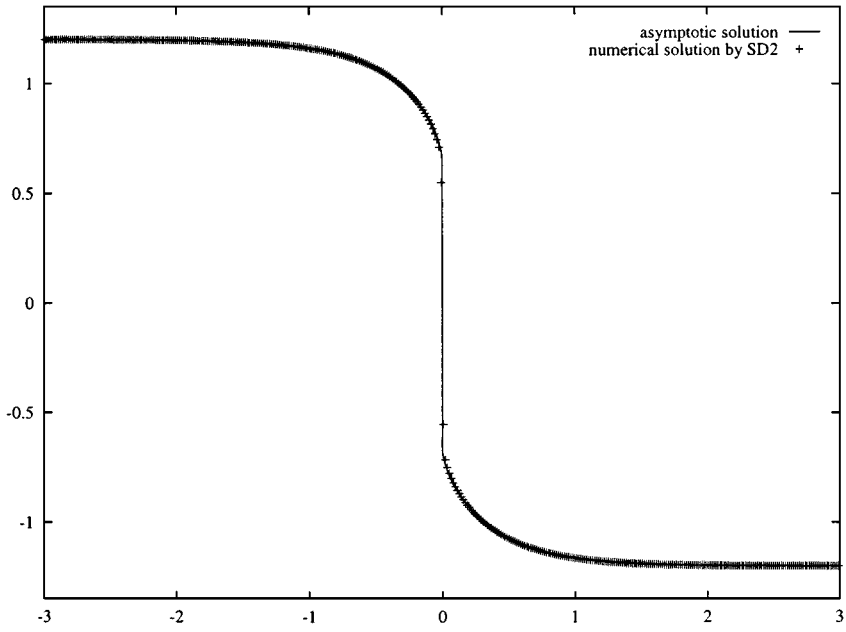

FIG. 6.21. Sharp resolution by the SD2 scheme. $N = 400$, $T = 1.5$.

We take ε to be 0.01, $f(u)$ to have an s-shaped form,

$$f(u) = \frac{u^2}{u^2 + (1-u)^2}, \tag{6.10}$$

and $v(u)$ to vanish at $u = 0, 1$,

$$v(u) = 4u(1-u). \tag{6.11}$$

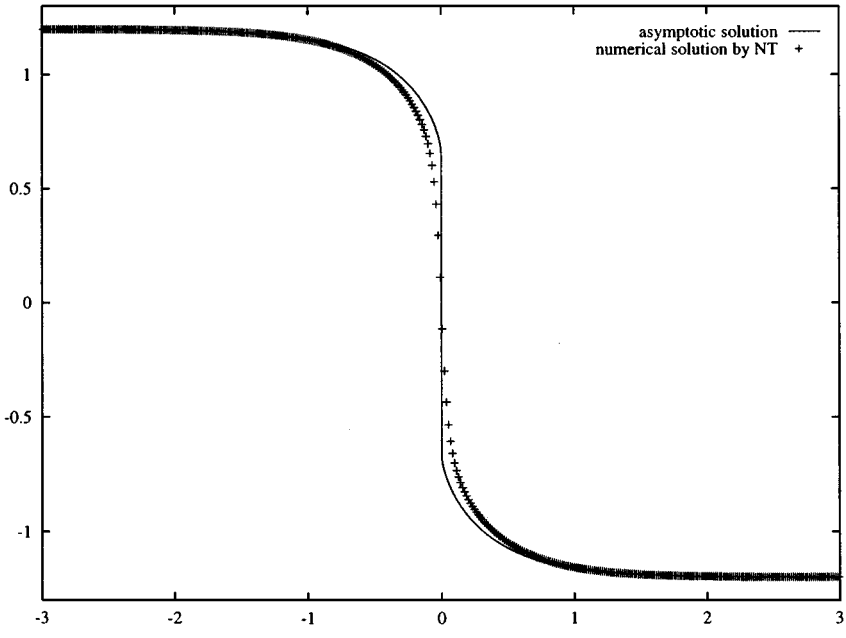

FIG. 6.22. Smeared discontinuity by the NT scheme. $N = 400$, $T = 1.5$.

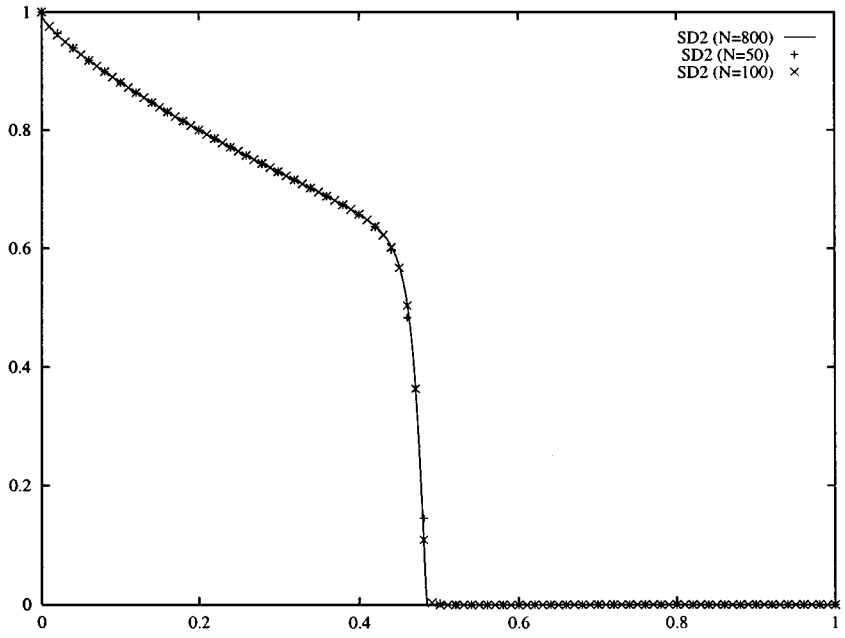

FIG. 6.23. Initial-boundary value problem (6.9)–(6.12). $T = 0.2$.

The initial function is

$$u(x,0) = \begin{cases} 1-3x, & 0 \le x \le \frac{1}{3}, \\ 0, & \frac{1}{3} < x \le 1, \end{cases} \tag{6.12}$$

the boundary value of $u(0,t) = 1$ is kept fixed.

The numerical solution computed by the SD2 scheme for different numbers of grid points is presented in Fig. 6.23. No exact solution to problem (6.9)–(6.12) is available, but if compared with the numerical solutions reported in [20], our solutions seem to converge to the correct entropy solution.

EXAMPLE 8 (Gravitational Effects). We now consider the Buckley–Leverett equation, (6.9), with the same $\varepsilon = 0.01$, the same diffusion coefficient, (6.11), and the flux function $f(u)$ including gravitational effects:

$$f(u) = \frac{u^2}{u^2 + (1-u)^2}(1 - 5(1-u)^2). \tag{6.13}$$

This equation is more complicated than the previous one since we should handle the flux (6.13) where $f'(u)$ changes sign. The numerical solutions to this equation and to Eqs. (6.9)–(6.11) subject to the Riemann initial data,

$$u(x,0) = \begin{cases} 0, & 0 \le x < 1 - \frac{1}{\sqrt{2}}, \\ 1, & 1 - \frac{1}{\sqrt{2}} \le x \le 1, \end{cases}$$

are shown in Fig. 6.24. It can be observed that our semi-discrete scheme provides the same high quality of numerical solutions for both of these problems.

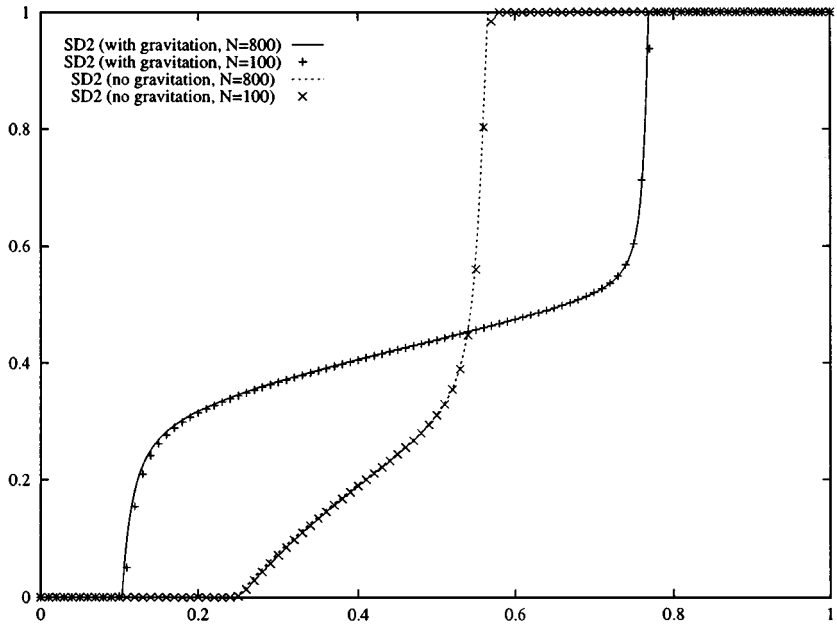

FIG. 6.24. Riemann problem for the Buckley–Leverett equation with and without gravitation. $T = 0.2$.

EXAMPLE 9 (Glacier Growth Model). In this example we consider a one-dimensional model for glacier growth (see [9, 21]). Let a glacier of height $h(x, t)$ rest upon a flat mountain. Its evolution is described by the nonhomogenious convection–diffusion equation

$$h_t + f(h)_x = \varepsilon(\nu(h)h_x)_x + S(x, t, h). \tag{6.14}$$

Let $\varepsilon = 0.01$. The typical flux and diffusion coefficient are

$$f(h) = \frac{h + 3h^6}{4}, \qquad \nu(h) = 3h^6. \tag{6.15}$$

We first look at the Riemann problem with

$$h(x, 0) = \begin{cases} 1, & x < 0, \\ 0, & x > 0, \end{cases}$$

that describes an outlet into a valley disregarding seasonal variations. To complete this simple model we use the source $S(x, t, h) = S_0(x)$ if $h(x, t) > 0$, and $S(x, t, h) = \max\{S_0(x), 0\}$ if $h(x, t) = 0$, where

$$S_0(x) = \begin{cases} 0, & x < -0.4, \\ \frac{1}{2}(x + 0.4), & -0.4 \le x \le -0.2, \\ -\frac{1}{2}x, & x > -0.2. \end{cases}$$

The numerical simulations for different number of grid points and at different times are presented in Figs. 6.25–6.27. These solutions, obtained by our SD2 scheme, seem to be more accurate than the solutions obtained by the operator splitting method in [21].

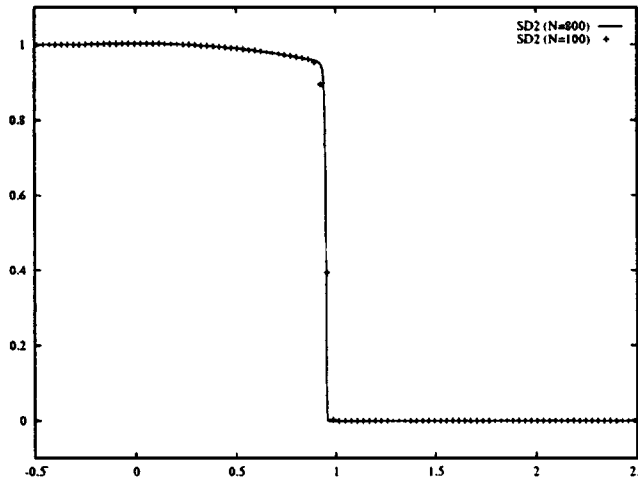

FIG. 6.25. Moving glacier at $T = 1$.

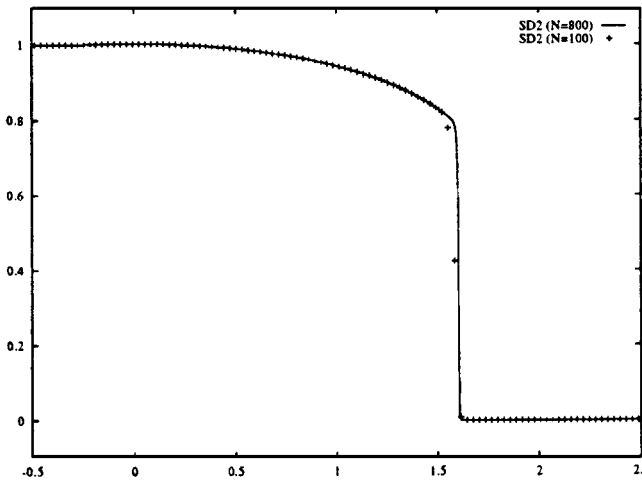

FIG. 6.26. Moving glacier at $T = 2$.

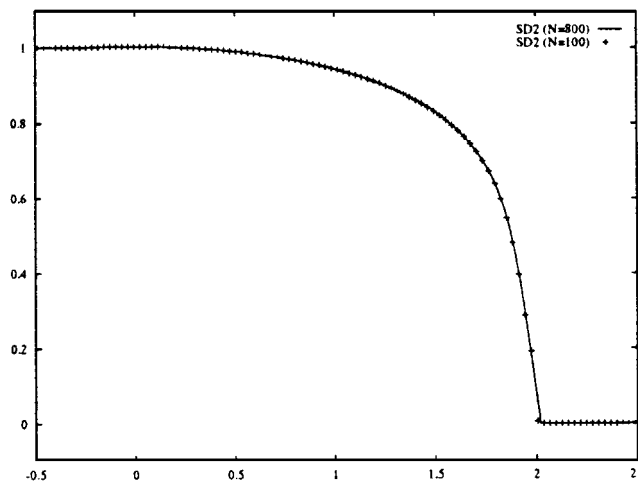

FIG. 6.27. Moving glacier at $T = 4$.

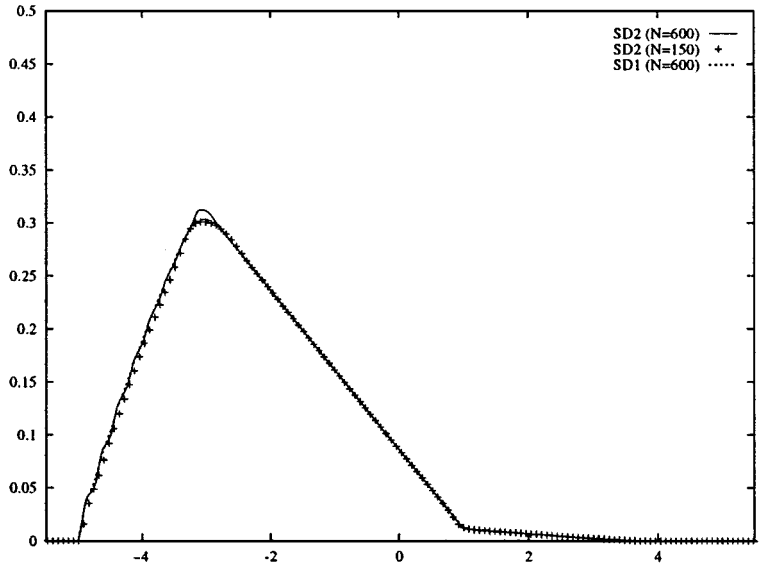

FIG. 6.28. Growing glacier at $T = 7.5$.

Second, we look at the growth of a new glacier ($h(x, 0) \equiv 0$). Let the glacier be restricted to the interval $[-5, 5]$. Then an appropriate source term is

$$S(x,t) = \begin{cases} 0, & x \le -5, \\ -0.01x + 0.05\sin(2\pi t), & x > -5. \end{cases}$$

Here the second, trigonometric term models seasonal variations.

Figures 6.28–6.33 illustrate the glacier growth computed by the Rusanov first-order and by our second-order semi-discrete schemes, SD1 and SD2, with different numbers of grid

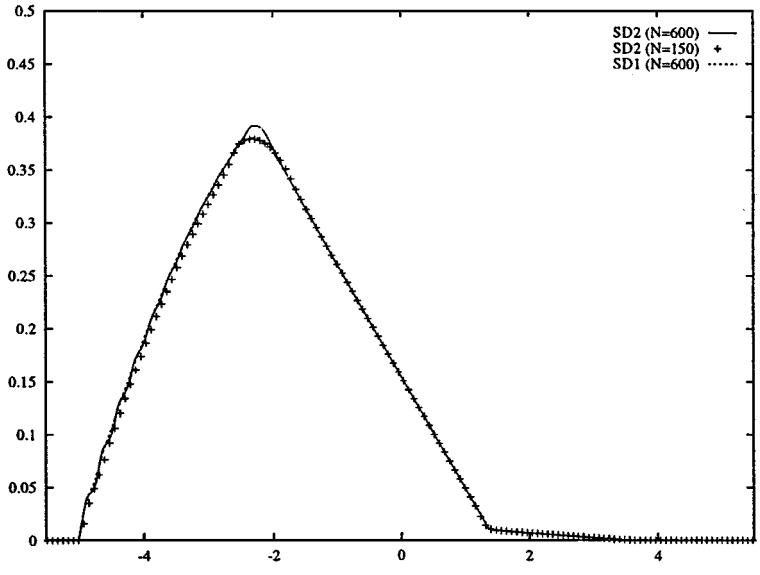

FIG. 6.29. Growing glacier at $T = 10.5$.

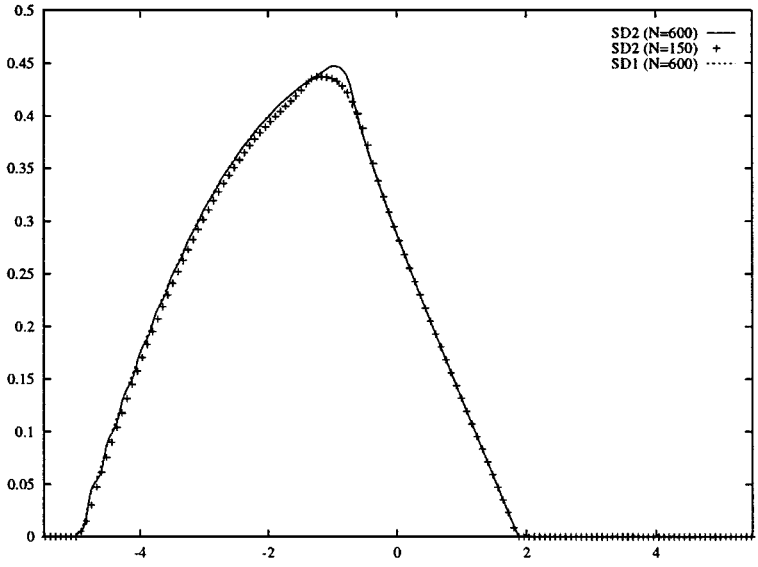

FIG. 6.30. Growing glacier at $T = 15$.

points. The SD2 scheme provides more accurate resolution of the upstream front, but admits some oscillations on the glacier downstream. The amplitude of these oscillations remains small but does not diminish with the grid refinement. Moreover, they tend to propagate up to the top of the glacier as N increases. At the same time, applying the SD1 scheme with a large number of grid points gives a very accurate, nonoscillatory solution, comparable with the one reported in [21].

EXAMPLE 10 (Hyperbolic–Parabolic Equation). We conclude this subsection with an example of strongly degenerate parabolic (or, hyperbolic–parabolic) convection–diffusion

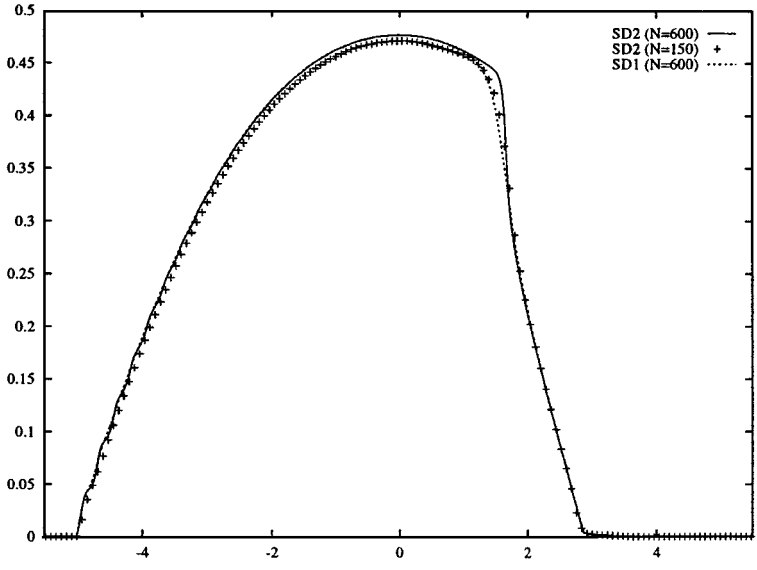

FIG. 6.31. Growing glacier at $T = 22.5$.

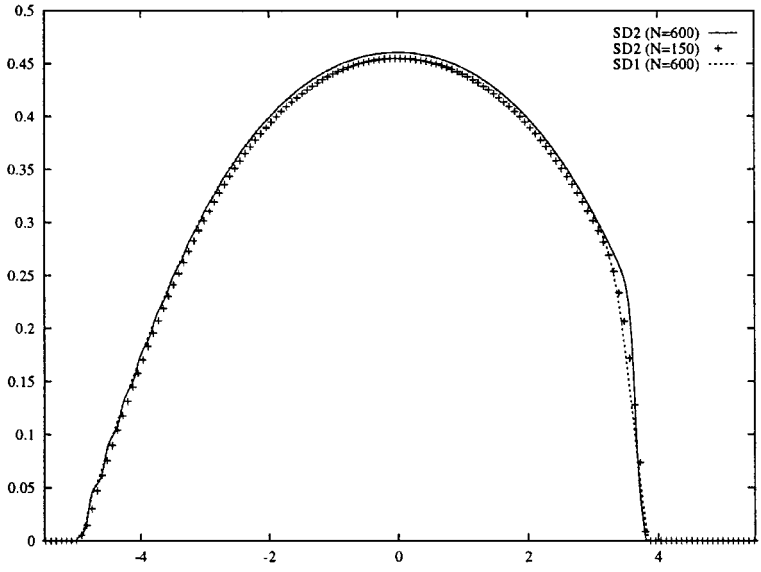

FIG. 6.32. Growing glacier at $T = 30$.

equation. Consider Eq. (6.9) with $\varepsilon = 0.1,\ f(u) = u^2$, and

$$v(u) = \begin{cases} 0, & |u| \le 0.25, \\ 1, & |u| > 0.25. \end{cases} \tag{6.16}$$

This $v(u)$ is a discontinuous function, and the equation is therefore of hyperbolic nature when $u \in [-0.25, 0.25]$ and parabolic elsewhere.

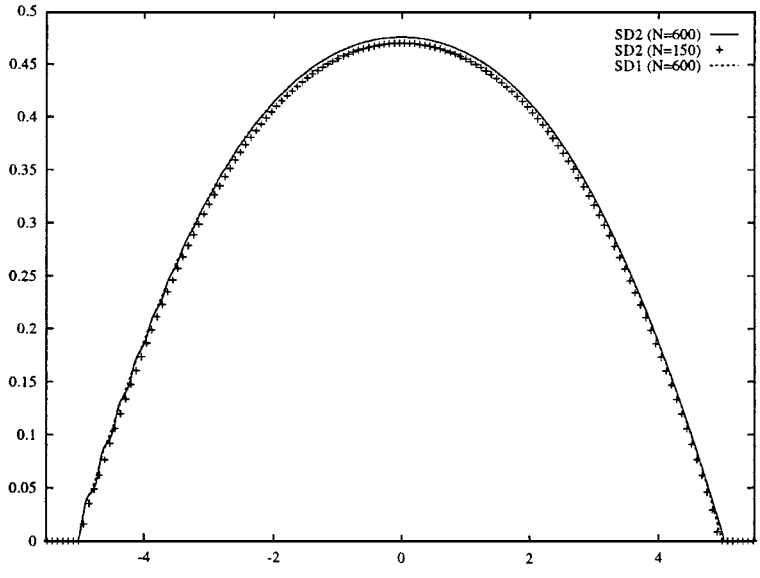

FIG. 6.33. Growing glacier at $T = 37.5$.

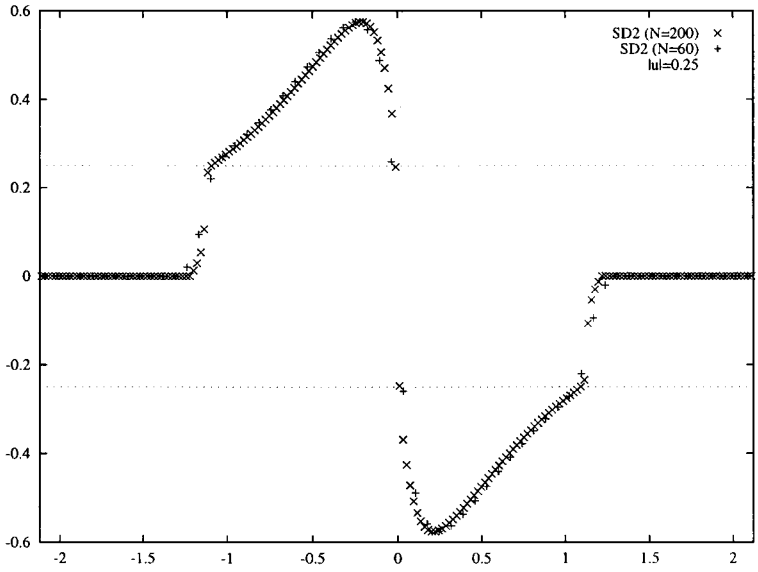

FIG. 6.34. Initial value problem (6.9), (6.16), (6.17). $T = 0.7$.

We apply our SD2 scheme to Eqs. (6.9), (6.16) subject to the initial data,

$$u(x,0) = \begin{cases} 1, & -\frac{1}{\sqrt{2}} - 0.4 < x < -\frac{1}{\sqrt{2}} + 0.4, \\ -1, & \frac{1}{\sqrt{2}} - 0.4 < x < \frac{1}{\sqrt{2}} + 0.4, \\ 0, & \text{otherwise.} \end{cases} \tag{6.17}$$

The results for two different number of grid points is shown in Fig. 6.34. We would like to point out the high resolution of discontinuities and the accurate transition between the hyperbolic and parabolic regions.

6.5. *Two-Dimensional Problems*

EXAMPLE 11 (Two-Dimensional Burgers-Type Equations). Consider the two-dimensional extension of the equation from Example 10,

$$u_t + (u^2)_x + (u^2)_y = \varepsilon(\nu(u)u_x)_x + \varepsilon(\nu(u)u_y)_y. \tag{6.18}$$

The numerical results obtained by our SD2 scheme are presented in Figs. 6.35 and 6.36. In these examples $\varepsilon = 0.1$; $\nu(u)$ is given by (6.16) (strongly degenerate parabolic problem)

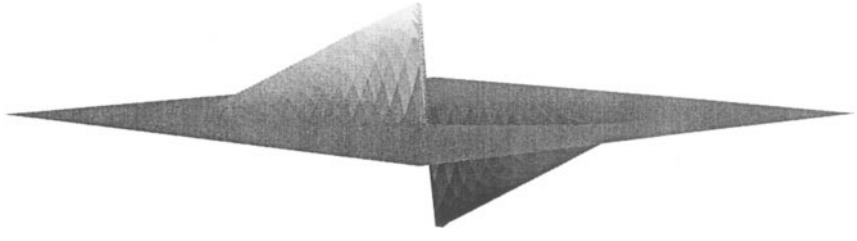

FIG. 6.35. Pure hyperbolic problem—solution at time $T = 0.5$ on a $60 * 60$ grid.

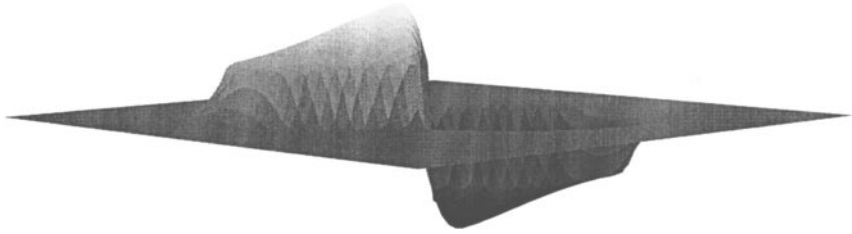

FIG. 6.36. Degenerate parabolic problem—solution at time $T = 0.5$ on a $60 * 60$ grid.

or $\nu(u) = 0$ (hyperbolic problem). The initial data are equal to -1 and 1 inside two circles of radius 0.4 centered at (0.5, 0.5) and $(-0.5, -0.5)$, respectively, and zero elsewhere inside the square $[-1.5, 1.5] \times [-1.5, 1.5]$. As in the one-dimensional examples, our scheme performs well in both hyperbolic and hyperbolic–parabolic cases even with relatively small number of grid points.

EXAMPLE 12 (Two-Dimensional Buckley–Leverett Equation). Finally, we solve the two-dimensional convection–diffusion equation

$$u_t + f(u)_x + g(u)_y = \varepsilon(u_{xx} + u_{yy}), \tag{6.19}$$

with $\varepsilon = 0.01$, the flux function of the form

$$\begin{aligned} f(u) &= \frac{u^2}{(u^2 + (1-u)^2)}, \\ g(u) &= f(u)(1 - 5(1-u)^2), \end{aligned} \tag{6.20}$$

and the initial data

$$u(x, y, 0) = \begin{cases} 1, & x^2 + y^2 < 0.5, \\ 0, & \text{otherwise.} \end{cases} \tag{6.21}$$

Note that the above model includes gravitational effects in the y-direction.

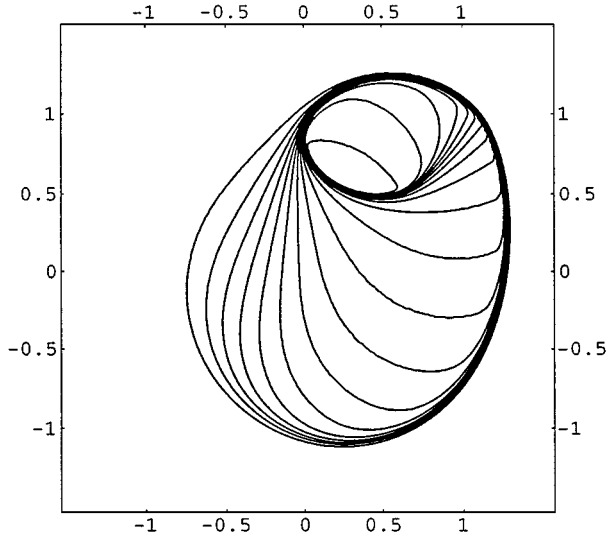

FIG. 6.37. Problem (6.19)–(6.21)—solution at time $T = 0.5$ on a $200 * 200$ grid.

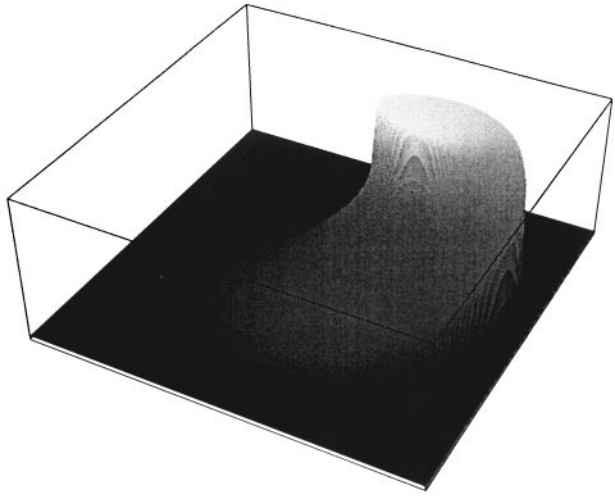

FIG. 6.38. Problem (6.19)–(6.21)—solution at time $T = 0.5$ on a $100 * 100$ grid.

The solution, computed in the domain $[-1.5, 1.5] \times [-1.5, 1.5]$ by the SD2 scheme, is shown in Figs. 6.37 and 6.38. Our scheme also provides a highly satisfactory approximation to this model with a nonlinear, degenerate diffusion.

ACKNOWLEDGMENT

The authors thank Dr. A. Medovikov (Institute of Numerical Mathematics, Russian Academy of Sciences, Russia) for a number of useful discussions and for providing his ODE solver DUMKA3. The work of A. Kurganov was supported in part by the NSF Group Infrastructure Grant. The work of E. Tadmor was supported in part by NSF Grant DMS97-06827 and ONR Grant N00014-91-J-1076.

REFERENCES

1. A. M. Anile, V. Romano, and G. Russo, Extended hydrodynamical model of carrier transport in semiconductors, *SIAM J. Appl. Math.*, in press.
2. P. Arminjon, D. Stanescu, and M.-C. Viallon, A two-dimensional finite volume extension of the Lax–Friedrichs and Nessyahu–Tadmor schemes for compressible flow, in *Proc. 6th Int. Symp. on CFD, Lake Tahoe, 1995*, M. Hafez and K. Oshima, editors, Vol. IV, pp. 7–14.
3. P. Arminjon and M.-C. Viallon, Généralisation du schéma de Nessyahu–Tadmor pour une équation hyperbolique à deux dimensions d'espace, *C. R. Acad. Sci. Paris Sér. I* **320**, 85 (1995).
4. F. Bianco, G. Puppo, and G. Russo, High order central schemes for hyperbolic systems of conservation laws, *SIAM J. Sci. Comput.* **21**, 294 (1999).
5. P. Colella, private communication.
6. H. K. Dahle, *Adaptive Characteristic Operator Splitting Techniques for Convection-Dominated Diffusion Problems in One and Two Space Dimensions*, Ph.D. thesis, University of Bergen, Norway, 1988.
7. B. Engquist and O. Runborg, Multi-phase computations in geometrical optics, *J. Comput. Appl. Math.* **74**, 175 (1996).

8. S. Evje, K. H. Karlsen, K.-A. Lie, and N. H. Risebro, Front tracking and operator splitting for nonlinear degenerate convection–diffusion equations, Institut Mittag-Leffler Report, Stockholm, Sweden, 1997.
9. A. C. Fowler, Glaciers and ice sheets, in *The Mathematics of Models for Climatology and Environment*, edited by J. I. Diaz, NATO ASI Series, Vol. 48 (Springer-Verlag, Berlin/New York, 1996), p. 302.
10. K. O. Friedrichs, Symmetric hyperbolic linear differential equations, *Comm. Pure Appl. Math.* **7**, 345 (1954).
11. S. K. Godunov, A finite difference method for the numerical computation of discontinuous solutions of the equations of fluid dynamics, *Mat. Sb.* **47**, 271 (1959).
12. J. Goodman, A. Kurganov, and P. Rosenau, Breakdown of Burgers-type equations with saturating dissipation fluxes, *Nonlinearity* **12**, 247 (1999).
13. A. Harten, High resolution schemes for hyperbolic conservation laws, *J. Comput. Phys.* **49**, 357 (1983).
14. A. Harten, B. Engquist, S. Osher, and S. R. Chakravarthy, Uniformly high order accurate essentially non-oscillatory schemes, III, *J. Comput. Phys.* **71**, 231 (1987).
15. A. Harten, P. D. Lax, and B. van Leer, On upstream differencing and Godunov-type schemes for hyperbolic conservation laws, *SIAM Rev.* **25**, 35 (1983).
16. A. Jameson, *Internat. J. Comput. Fluid Dynamics* **4**, 171 (1995); **5**, 1 (1995).
17. G.-S. Jiang, D. Levy, C.-T. Lin, S. Osher, and E. Tadmor, High-resolution non-oscillatory central schemes with non-staggered grids for hyperbolic conservation laws, *SIAM J. Numer. Anal.* **35**, 2147 (1998).
18. G.-S. Jiang and E. Tadmor, Non-oscillatory central schemes for multidimensional hyperbolic conservation laws, *SIAM J. Sci. Comput.* **19**, 1892 (1998).
19. S. Jin and Z. Xin, The relaxation schemes for hyperbolic systems of conservation laws in arbitrary space dimensions, *CPAM* **48**, 235 (1995).
20. K. H. Karlsen, K. Brusdal, H. K. Dahle, S. Evje, and K.-A. Lie, The corrected operator splitting approach applied to a nonlinear advection–diffusion problem, *Comput. Methods Appl. Mech. Eng.* **167**, 239 (1998).
21. K. H. Karlsen and K.-A. Lie, An unconditionally stable splitting for a class of nonlinear parabolic equations, *IMA J. Numer. Anal.* **19**, 609 (1999).
22. K. H. Karlsen and N. H. Risebro, An operator splitting method for nonlinear convection–diffusion equations, *Numer. Math.* **77**, 365 (1997).
23. K. H. Karlsen and N. H. Risebro, Corrected operator splitting for nonlinear parabolic equations, *SIAM J. Numer. Anal.* **37**, 980 (2000).
24. R. Kupferman, Simulation of viscoelastic fluids: Couette–Taylor flow, *J. Comput. Phys.*, to appear.
25. R. Kupferman, A numerical study of the axisymmetric Couette–Taylor problem using a fast high-resolution second-order central scheme, *SIAM J. Sci. Comput.* **20**, 858 (1998).
26. R. Kupferman and E. Tadmor, A fast high-resolution second-order central scheme for incompressible flows, *Proc. Nat. Acad. Sci.* **94**, 4848 (1997).
27. A. Kurganov, *Conservation Laws: Stability of Numerical Approximations and Nonlinear Regularization*, Ph.D. thesis, Tel-Aviv University, Israel, 1997.
28. A. Kurganov and P. Rosenau, Effects of a saturating dissipation in Burgers-type equations, *Comm. Pure Appl. Math.* **50**, 753 (1997).
29. P. D. Lax, Weak solutions of nonlinear hyperbolic equations and their numerical computation, *Comm. Pure Appl. Math.* **7**, 159 (1954).
30. B. van Leer, Towards the ultimate conservative difference scheme. III. Upstream-centered finite-difference schemes for ideal compressible flow, *J. Comput. Phys.* **23**, 263 (1977).
31. B. van Leer, Towards the ultimate conservative difference scheme. V. A second order sequel to Godunov's method, *J. Comput. Phys.* **32**, 101 (1979).
32. D. Levy, G. Puppo, and G. Russo, Central WENO schemes for hyperbolic systems of conservation laws, *Math. Model. Numer. Anal.* **33**, 547 (1999).
33. D. Levy and E. Tadmor, Non-oscillatory central schemes for the incompressible 2-D Euler equations, *Math. Res. Lett.* **4**, 1 (1997).
34. X.-D. Liu and P. D. Lax, Positive schemes for solving multidimensional systems of hyperbolic conservation laws, *Comput. Fluid Dynamics J.* **5**, 1 (1996).

35. X.-D. Liu and S. Osher, Convex ENO high order multi-dimensional schemes without field by field decomposition or staggered grids, *J. Comput. Phys.* **142**, 304 (1998).
36. X.-D. Liu and E. Tadmor, Third order nonoscillatory central scheme for hyperbolic conservation laws, *Numer. Math.* **79**, 397 (1998).
37. A. A. Medovikov, High order explicit methods for parabolic equations, *BIT* **38**, 372 (1998).
38. H. Nessyahu and E. Tadmor, Non-oscillatory central differencing for hyperbolic conservation laws, *J. Comput. Phys.* **87**, 408 (1990).
39. H. Nessyahu and E. Tadmor, The convergence rate of approximate solutions for non-linear scalar conservation laws, *SIAM J. Numer. Anal.* **29**, 1505 (1992).
40. S. Osher, Convergence of generalized MUSCL schemes, *SINUM* **22**, 947 (1984).
41. S. Osher and E. Tadmor, On the convergence of difference approximations to scalar conservation laws, *Math. Comput.* **50**, 19 (1988).
42. P. Roe, Approximate Riemann solvers, parameter vectors, and difference schemes, *J. Comput. Phys.* **43**, 357 (1981).
43. V. Romano and G. Russo, Numerical solution for hydrodynamical models of semiconductors, M^3AS, preprint.
44. C.-W. Shu, Total-variation-diminishing time discretizations, *SISSC* **6**, 1073 (1988).
45. C.-W. Shu and S. Osher, Efficient implementation of essentially non-oscillatory shock-capturing schemes, *J. Comput. Phys.* **77**, 439 (1988).
46. G. Sod, A survey of several finite difference methods for systems of nonlinear hyperbolic conservation laws, *J. Comput. Phys.* **22**, 1 (1978).
47. E. Tadmor, Convenient total variation diminishing conditions for nonlinear difference schemes, *SIAM J. Numer. Anal.* **25**, 1002 (1988).